# CHAPTER 5

# Imaging in Depth: Controversies and Opportunities

**Don O'Malley**

Department of Biology
Northeastern University
Boston, Massachusetts 02115



METHODS IN CELL BIOLOGY, VOL. 89


0091-679X/08 $35.00
DOI: 10.1016/S0091-679X(08)00605-5

## Abstract

One enduring challenge of biological imaging is achieving *depth of penetration*—into cells, tissues, and animals. How deeply can we probe and with what resolution and efficacy? These are critical issues as microscopists seek to push ever deeper, while resolving structural details and observing specific molecular events. In this guide to depth-appropriate modalities, standard optical platforms such as confocal and two-photon microscopes are considered along with complementary imaging modalities that range in depth of penetration. After an introduction to basic techniques, the trade-offs and limitations that distinguish competing technologies are considered, with emphasis on the visualization of subcellular structures and dynamic events. Not surprisingly, there are differences of opinion regarding imaging technologies, as highlighted in a section on point-scanning and Nipkow-disk style confocal microscopes. Confocal microscopy is then contrasted with deconvolution and multi-photon imaging modalities. It is also important to consider the detectors used by current instruments (such as PMTs and CCD cameras). Ultimately specimen properties, in conjunction with instrumentation, determine the depth at which subcellular operations and larger-scale biological processes can be visualized. Relative advantages are mentioned in the context of experiment planning and instrument-purchase decisions. Given the rate at which new optical techniques are being invented, this report should be viewed as a snapshot of current capabilities, with the goal of providing a framework for thinking about new developments.

## I. Introduction

Biological imaging spans the scale from atomic-level, cryoEM reconstructions to whole-animal imaging (not counting satellite imaging of ecosystems!). Ultimately, the goal is to look deeply, dynamically, and with molecular specificity. While this "holy grail" remains elusive, the nexus of new tools and probes is producing remarkable gains. With the advent of genetic tools for the manipulation and imaging of cells, tissues, and animals (Bhaumik and Gambhir, 2002; Cubitt *et al.*, 1995; Higashijima *et al.*, 2000; Nasevicius and Ekker, 2000; Perkins *et al.*, 2002), light microscopy has been delving into myriad new frontiers. Biologists are able to image living specimens more deeply and with greater resolution by employing an increasingly powerful range of tools and technologies (Beis and Stainier, 2006; Cox *et al.*, 2000; Denk and Svoboda, 1997; Gahtan and Baier, 2004; Göbel *et al.*, 2007; Holtmaat *et al.*, 2005; Iyer *et al.*, 2006; Jontes *et al.*, 2000; Kerr *et al.*, 2005; Kuo *et al.*, 2007; Livet *et al.*, 2007; O'Malley *et al.*, 2003; Orger *et al.*, 2008; Shcherbo *et al.*, 2007). Which technique should be chosen, however, and which specific instrument should be employed, depend critically upon the experimental question being asked. This guide mentions a broad range of important techniques,

but the focus is on a smaller set of imaging modalities and their defining features, including instrumentation particulars and the underlying optical physics. Techniques are emphasized that provide details at the molecular, subcellular, and cellular levels, often within the context of larger cell assemblies inside living animals. By such imaging methods and optical manipulations, structures and processes previously occult to biologists can now be grasped. These technologies are ordered along the dimension of depth of penetration. Experimental results that illuminate key capabilities of these different imaging options are emphasized. While there are many powerful imaging modalities, this guide will focus mainly on three: confocal, two-photon, and deconvolution microscopy. But before getting into the depths of biological imaging, some mention of the visualization techniques used at the finest scales of biological structure is in order.

## A. Imaging at the Atomic Level

At the nanometer scale, molecules and even individual atoms can be imaged and often resolved using atomic force microscopy (AFM) and/or electron microscopy (EM). AFM is one of a number of "near-field" imaging techniques where a mechanical imaging probe comes into contact with a sample (Ando *et al*., 2007; Frankel *et al*., 2006; Hansma and Hoh, 1994; Kellermayer *et al*., 2006). X-ray diffraction and cryoEM techniques provide atomic-scale views into the structure of macromolecules (see, e.g., Frangakis and Förster, 2004; Jiang and Ludtke, 2005; Koster and Klumperman, 2003; Wu *et al*., 2000), but they also pose significant demands in terms of sample purification and preparation, and are generally not suitable for live specimen imaging (but see Ackerley *et al*., 2006). While the near-field techniques examine surface structures via different means of probe–sample interaction, they are depth-limited, in general terms, to the surface of the sample—often the plasma membrane of a cell. In particular, AFM provides high-resolution views of biological surfaces such as the upper membrane of cells cultured in monolayers. A complementary technique, total internal reflectance fluorescence microscopy (TIRF), produces a detailed "bottom view" in that the specimen is typically resting on a coverslip and viewed from below. TIRF examines a region that extends for 100 nm or so into the tissue adjacent to the coverslip (Axelrod, 2003). Collectively these techniques provide fine molecular-level and/or topographic details of biological structures, which are necessary for piecing together the higher-level functioning of cells. Tissues and organisms, however, are thicker conglomerates of molecular devices and cell assemblies. To understand the organization and physiology of these structures one needs to image in greater depth and with resolution sufficient to characterize the biological processes of interest. In this guide, consideration is given to the range of optical tools and imaging approaches that can be employed across the scale of "depths" at which one would like to probe biological structures.

## II. Basic Imaging Methodologies

### A. Light and Fluorescence Microscopy

Light microscopy has myriad applications across the realms of biology, biotechnology, and medicine. Staining techniques are the staple of clinical histology labs (Bancroft and Gamble, 2001), illustrating the ageless value of the workhorse of biological imaging, the compound light microscope. Past innovations in light microscopy included phase contrast and differential interference contrast (DIC), both of which allow unstained (including living) specimens to be seen in far better detail due to enhanced contrast (Cox, 2007; Sluder and Wolf, 2007). With fluorescence techniques, one has the ability to visualize structures with molecular specificity using both traditional fluorophores (Taylor and Salmon, 1989) and genetically encoded fluorophores (Cubitt *et al*., 1995; Lippincott-Schwartz and Patterson, 2003; Shcherbo *et al*., 2007). The conjunction of fluorescent probe advances and newer imaging modalities (such as confocal and two-photon) is at the heart of the biological imaging revolution of the past 20 years. Adding to this imaging frenzy are higher-resolution light-microscopic techniques that improve spatial resolution well beyond the Abbé diffraction limit (Egner *et al*., 2002a; Hell, 2007). One technique called STORM relies on the photoswitching of fluorophores to achieve nanometer scale resolution (Rust *et al*., 2006). Perhaps the most advanced of these techniques is stimulated emission-depletion (STED) (Hell and Wichmann, 1994), which enables the resolution of nanometer scale structures within fluorescently labeled cells (also see article by S. Hess, this volume). STED has been effectively employed in double-labeling experiments (Donnert *et al*., 2007a), and has also revealed the dynamics of syntaxin protein clusters in living cells (Sieber *et al*., 2007; Willig *et al*., 2006). This was accomplished using a custom stage-scanning microscope, but if this approach becomes more widely available, it offers perhaps the highest resolution for imaging structures throughout the three-dimensional (3D) thickness of living cells. At present, the extent to which such "super-resolution" techniques can be pushed deeper into living tissues and intact animals is unclear.

### B. TIRF Microscopy

Of the optical imaging techniques, TIRF is at the bottom of the depth-of-penetration list, both figuratively and literally. TIRF depends upon acute angular illumination of (usually) the bottom of a coverslip such that (1) all of the incident illumination is reflected off the interface and (2) the only illumination of the sample is due to the penetration of an evanescent wave through the coverslip and into the sample (reviewed by Axelrod, 2003; also see Axelrod, this volume). This limits TIRF illumination to a depth of roughly 100 nm, that is to just a small fraction of the thickness of a eukaryotic cell. What TIRF gains in return is the ability to better visualize near-surface structures and attachments to the substrate, which are of

interest in multiple areas of biomedical research (see, e.g., Bos and Kleijn, 1995; Ferko *et al*., 2007; Lassen and Malmsten, 1996; Partridge and Marcantonio, 2006; Reichert and Truskey, 1990). While AFM and TIRF are wholly unrelated techniques, they both provide perimembrane views of the cell (from the top and bottom surfaces, respectively). AFM's mechanical approach is in some fashion ''rougher'' than the gentler touch of TIRF's photons, but more important is their complementary nature: TIRF, like other fluorescence modalities, offers potentially tremendous molecular specificity (determined by the specificity of the fluorescent probe), whereas AFM provides general structural context. In addition, TIRF can visualize dynamic events occurring just under the membrane such as the docking and fusion of secretory granules (Ohara-Imaizumi *et al*., 2004). Because TIRF penetrates so shallowly into the cell, this gives it a very thin optical section—perhaps the thinnest of any optical technique.

## C. DIC Microscopy

In contrast to TIRF and AFM, DIC imaging offers the ability to look through cells and groups of cells, and depending on size and opacity, through whole living organisms. Working with unstained specimens, it generates contrast that can be greatly enhanced via analog and/or digital signal processing (Salmon and Tran, 1998; Sluder and Wolf, 2007). DIC also produces better resolution than the more commonly available *phase contrast* imaging modality because of the higher numerical aperture of DIC illumination; see Cox (2007) for a succinct explanation of these imaging modalities. In regards to DIC's depth of penetration, it is similarly susceptible to influences that hinder conventional bright field and fluorescence microscopy, variously: opacity, turbidity, or light scattering. Nonetheless, DIC is useful for a variety of specimens including unstained cells, tissue sections, and living animals (Dahm *et al*., 2007). One modification that improved the useful depth of DIC imaging was the use of infrared (IR) illumination (Dodt and Zieglgansberger, 1990). The greater penetration of IR light into biological tissues has led to its widespread use in electrophysiological experiments on brain slices (Bagnall *et al*., 2007; Jagger and Housley, 2003; Stuart *et al*., 1993; Wang *et al*., 2003).

The ultimate depths attained with DIC vary based upon both specimen characteristics and the specific details of the DIC implementation. While suitable imaging details were initially reported for depths of 50–100 $\mu$m in rat brain slices (Stuart *et al*., 1993), cell bodies may be visualized with IR-DIC up to 200 $\mu$m deep. Attention to such details as (1) perfusion of the animal with ice-cold saline prior to dissection, (2) choice of camera (e.g., Dage IR-1000), and (3) viewing method, for example via direct connection of the camera to a black and white TV monitor, can make a big difference in the ultimate performance of IR-DIC (Peter Saggau, personal communication). While such depths attained by DIC rival or even surpass those attainable with confocal microscopy, this would be situation dependent. A very bright GFP-labeled cell may be detected (in slices of rat brainstem), even with conventional fluorescence optics, at depths deeper than those where DIC is

able to reveal the structural details necessary for visually guided patch clamping (C-J. Yu and J. Gnadt, personal communication). Under favorable conditions, DIC does produce the finest optical sectioning capability of any "whole-cell" imaging approach, with an optical section thickness as narrow as 0.3 $\mu$m. The only method that produces superior whole-cell, $z$-axis image resolution is the physical cutting of very thin sections, which can then be stained and viewed by various imaging modalities, including light and electron microscopy.

Earlier we related AFM to TIRF as conveying structural details versus molecular specificity in regards to the specimen's surface. A similar relationship exists between confocal microscopy (discussed below) and DIC wherein both are able to look through cells (and deeper into tissues) while providing complementary details: structural for DIC, molecular for confocal fluorescence images. DIC is often the method of choice for unstained specimens (see, e.g., Concha and Adams, 1998; Dahm *et al.*, 2007) and it is often possible to record the same microscopic field of view with both DIC and confocal. As such, DIC can provide structural context within which to interpret fluorescent objects. But there can be issues if one wishes to acquire both DIC and fluorescence images without switching microscope objectives. While Nomarski-style DIC objectives are preferable in this respect, there is still significant loss of the fluorescence signal. One may encounter further complications with fiber-coupled confocal microscopes due to the varying ellipticity of polarization of laser light (Amos *et al.*, 2003). In instances where the DIC and confocal images cannot be suitably obtained with a single microscope objective, it then becomes necessary to rotate the microscope's objective turret. Because high-resolution imaging is often done with immersion objectives (e.g., oil or water), it is not trivial to swap objectives while maintaining a precisely registered field of view, so one should ascertain that both imaging modalities can be acquired together if image registration is important.

There are other developments in this area (Cody *et al.*, 2005). One promising approach is differential phase contrast (DPC) microscopy, which is more compatible with confocal imaging and requires less illumination than DIC, but DPC has not achieved much attention, perhaps because the specimen cannot be directly viewed as it can with DIC (Amos *et al.*, 2003). While the different nuances discussed above may seem esoteric, they can critically shape the options available to investigators. Such issues are especially important when it comes to the purchase of expensive instruments by individual researchers or by core facilities. In proceeding through the next set of imaging modalities, such nuances are highlighted while addressing some of the opportunities, trade-offs, and controversies that swirl in the winds of the biological imaging frontier.

## III. Forays Deeper into Depth

To understand how confocal imaging (described in the next section) and other techniques have extended our view deeper into biological structures, we should first provide some important context. For starters, depth of penetration is entirely

contingent upon the optical properties of the specimen—how transparent, scattering, or opaque it is (Oheim *et al.*, 2001). With basic light microscopy, one might see entirely through tissues and even whole animals—depending on transparency (or translucency). In the case of zebrafish, one can see entirely through an embryo or larva with basic light and fluorescence microscopy. This transparency was a major factor in the organism's skyrocketing popularity over the past 15 years leading to its current entrenchment as a model organism in developmental genetics, neuroscience, and other areas (Detrich *et al.*, 2004). Conversely, the skull of mammals is so opaque that one can resolve little or no cellular detail within the cerebral cortex without first drilling holes. The opacity of brain tissue is itself variable depending both upon species (Cinelli, 2000) and upon age (Oheim *et al.*, 2001). Embryonic and neonatal rat thalamic slices, for example, are more easily peered into (with confocal) than are slices from adult rats (Zhou *et al.*, 1997). In the case of larval zebrafish, confocal imaging reveals synaptic-level details throughout the brain and spinal cord (Fetcho and O'Malley, 1995; Gahtan and O'Malley, 2003). This variability seems related to myelination and perhaps explains our ability to resolve fine neural structures throughout the 300 $\mu$m thickness of the larval zebrafish brain—while seeing little cellular detail 80 $\mu$m deep into an adult rat brain slice, even with confocal. Why brain translucency is so variable is not well defined, but even in the case of zebrafish, transparency is relative: Mutant lines have been made such as *nacre*, in which the larvae are almost glass-like in appearance (Lister *et al.*, 1999; O'Malley *et al.*, 2004).

So does one need a confocal microscope to look through the CNS of larval zebrafish? Not surprisingly, it depends on what one wishes to see. In a transgenic zebrafish line where the rod photopigment rhodopsin has been fused with green fluorescent protein, the now fluorescent photoreceptors are easily visualized in anesthetized larvae using a fluorescence dissecting microscope (Fig. 1A and B). The individual photoreceptors are not easily resolved (or counted) with the dissecting microscope, but with confocal (Fig. 1C–F), individual photoreceptors and subcellular details are resolved including the banding pattern of the GFP-rhodopsin protein in the outer segments (arrows in Fig. 1F). The instrumentation required thus depends upon the specific experimental needs: Fluorescence dissecting microscopes are becoming increasingly popular in the zebrafish community for screening embryos and larvae for fluorescence labeling (during genetic screens) and for taking low-resolution (but often deep-tissue) pictures. Conventional wide-field fluorescence microscopy can also be used for imaging neurons in larval zebrafish, but confocal microscopy becomes necessary for resolving the fine anatomical details needed to identify individual neurons in the larval spinal cord (Fetcho and O'Malley, 1995; Fetcho *et al.*, 1998; Hale *et al.*, 2001) and brainstem (Gahtan *et al.*, 2002; O'Malley *et al.*, 1996, 2003).

When it comes to mammalian brains, and many other animal tissues, the imaging conditions become less clear. The two-photon (or multi-photon) imaging technique (discussed below) often becomes necessary and David Piston speaks of a "6-fold rule" meaning that one can obtain comparable structural detail sixfold

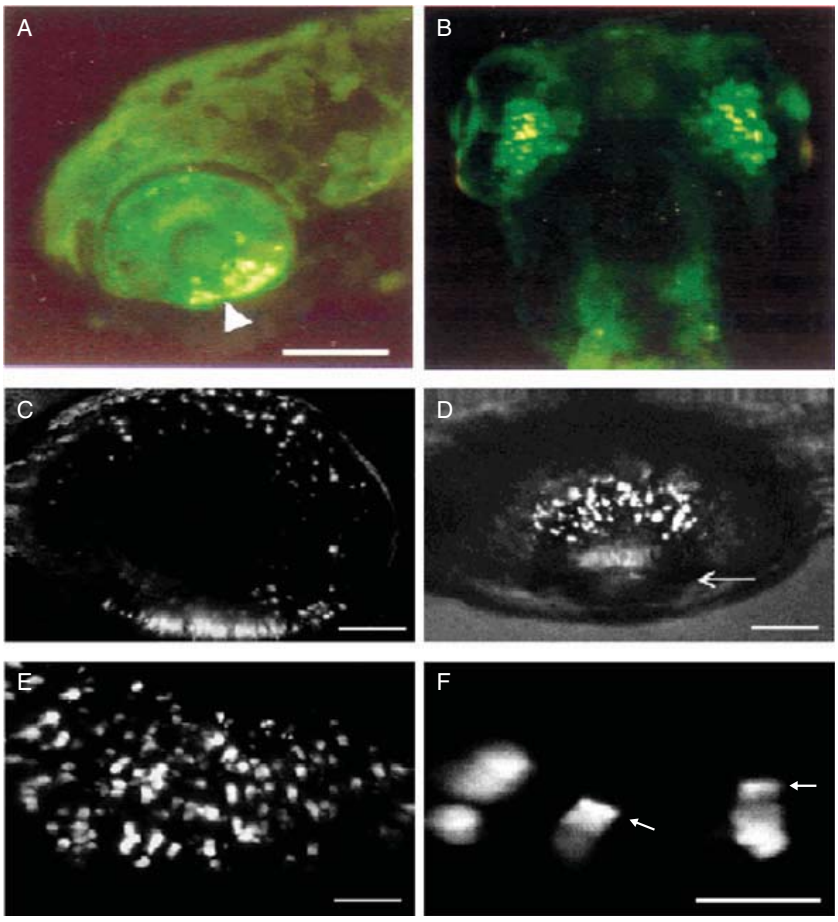


**Fig. 1** Photoreceptors in anesthetized zebrafish. Images are from transgenic larvae expressing GFP-rhodopsin fusion protein. (A, B) Fluorescent rod photoreceptors in ventral retina (arrowhead) are easily viewed using a fluorescence dissecting microscope. Confocal maximum projection images (C–F) show photoreceptors at higher resolution, revealing banding patterns in rod outer segments (arrows in F). Arrow in (D) shows location of lens. Scale bars = 150 $\mu$m (A, B); 50 $\mu$m (C, D); 25 $\mu$m (E); and 10 $\mu$m in (F). Reprinted with permission from *Visual Neuroscience* (from Perkins *et al*., 2002).

deeper with two-photon microscopes than with confocal microscopy; this is nicely illustrated using comparison confocal and two-photon images from shark choroid plexus (Piston, 2005). While an assortment of macroscopic imaging modalities enable peering through the entire bodies of animals (both small and large), two-photon represents the method of choice for resolving microscopic details *in vivo*. But two-photon is also the most expensive microscopic imaging modality and is often not available, so it is important to consider what one can do with the more widely available confocal methods, as well as with deconvolution methods that are available to anyone with a digital fluorescence microscope and an internet connection (Majewska *et al*., 2000).

## A. Confocal Microscopy: Basics

Confocal microscopy is (most commonly) a variant of fluorescence microscopy in which a simple optical trick is used to collect light from a narrow slice or ''optical section'' through a sample such as a cultured cell or intact animal. By selecting for photons that originate from a given focal plane, it provides superior resolution at tissue depths where wide-field fluorescence images become quite blurry. Confocal microscopic imaging was invented by Marvin Minsky in 1955 in his efforts to see more clearly the organization of the brain (Minsky, 1988). In trying to understand how to better resolve details of neural circuits from within brain tissue, Minsky reasoned that if one illuminated just a small point in a sample using a first pinhole in the illumination path (this is done more effectively today with lasers) and then collected light only from that point, using a second pinhole aperture in the image transmission path, then one could extract an optical section from a biological specimen. This ''double-focusing'' mechanism is described more familiarly today as the use of pinhole apertures in CONjugate FOCAL planes, wherein the term ''confocal'' actually derives (Sheppard and Choudhury, 1977). This is indeed the key element that defines the operation of the confocal microscope. Previously pinhole apertures had been used in spectroscopic studies (Naora, 1955), but Minsky was able to build a working (albeit crude) confocal microscope, in part by using a military surplus long-persistence radar scope.

The confocal technique enables acquisition of much narrower optical sections or optical slices through a specimen than is possible with wide-field (conventional) fluorescence microscopy. This allows one to peer deeper into tissues (within limits) and to pull detailed structures out of a fluorescent blur. The realization of commercially successful confocal imaging systems, however, would not occur until well into the 1980's. The Olympus Corporation web site (www.olympusfluoview.com) has put it thus: ''Fortuitously, shortly after Minsky's patent had expired, practical laser-scanning confocal microscope designs were translated into working instruments by several investigators.'' While the fortuitousness of this timing is perhaps subjective, the widespread commercialization of confocal technology depended upon the availability of computing systems both to control the instruments and to efficiently collect and utilize the large amounts of data generated. A far more detailed explanation of confocal microscopy is provided by the highly regarded Handbook of Biological Confocal Microscopy (Pawley, 2006); the historical realization of this instrument is described by Amos and White (2003).

## B. Confocal Microscopy: Competing Designs

In Minsky's original design, the specimen was scanned under the light source; this was also done in some of the earliest confocal images of biological specimens (Brakenhoff, 1979; Brakenhoff *et al*., 1985; Valkenburg *et al*., 1985), but the most common confocal instrument is referred to variously as a point-scanning, line-scanning or laser-scanning confocal microscope. Here, a diffraction-limited spot

from a laser beam is raster scanned across the specimen, building up an image point by point as the signal is detected by a photomultiplier tube (PMT). Even with rapid scanning mirrors, this process takes sufficient time as to pose trade-offs. This is indeed the most crucial difference between point-scanning confocals and their biggest competitor, the spinning-disk confocal which scans many points simultaneously and records data in parallel onto a CCD camera. While either variant works well for many applications, each has distinctive features that become magnified in the context of purchasing decisions. A third model is the "slit scanning" confocal which rapidly acquires images that are "confocal" along one dimension within the *xy* plane (Bembenek *et al.*, 2007; Gasparini *et al.*, 2007). A further variant is reflectance confocal which uses reflected rather than fluorescence light to perform confocal sectioning. Reflectance confocal is frequently used in clinical and preclinical applications (see, e.g., Collier *et al.*, 2007; Dwyer *et al.*, 2006; González and Tannous, 2002). More recently, spectral scanning has been employed to enable finer spectral resolution of signals emanating from the sample (reviewed in Dickinson *et al.*, 2001; Zimmermann *et al.*, 2003). Despite the many options available, point scanning and spinning disk are the confocal platforms most commonly used. They also provide a convenient framework within which to consider the performance limits of confocal microscopy.

Spinning-disk confocals (also known as Nipkow-disk or disk-scanning confocals) scan many points at once in a spiral pattern and can thus obtain 2D images of large areas considerably faster than point-scanning instruments. An ensuing and quite practical feature is that one can directly view the specimen when using such spinning-disk confocals. In contrast, on point-scanning confocals, the specimen is viewed on a TV or computer monitor. Spinning-disk models, however, have a significant drawback in that they lack a continuously adjustable aperture at the emission pinhole. Since the earliest commercial confocals (such as the BioRad MRC500), point-scanning confocals have often had this feature, since there is only one pinhole to adjust. This facilitates the imaging of live specimens because the degree of optical sectioning can be traded away, to an arbitrary extent, in exchange for often dramatically increased signal. This option to adjust or "open" the pinhole aperture has often aided the visualization of dynamic physiological processes (see, e.g., O'Malley *et al.*, 1996, 2003; O'Malley, 1994; Yu *et al.*, 1994; Zhou *et al.*, 1997). Because the greater signal passing through the open aperture may allow for a substantial reduction in the illumination intensity, this can reduce two of the most serious limiting factors in fluorescence microscopy—photodamage and photobleaching (Donnert *et al.*, 2007b). With point scanners, once the physiological data are acquired, the aperture can be narrowed, and the laser intensity increased, to record finer anatomical details. In principle, the Nipkow-disk design might circumvent this limitation by providing a set of interchangeable disks with a good range of aperture settings. While there are efforts in this direction, the utility of such an approach remains to be documented.

The differences in confocal design come into play in a variety of confocal applications. For example, point-scanning instruments are easily employed in

diverse experiments where photo-manipulation is applied to precise locations on a biological specimen. Experiments in the area of FRAP (fluorescence recovery after photobleach; Braeckmans *et al.*, 2007; Klein *et al.*, 2003), photoactivation (Chudakov *et al.*, 2006), laser-ablation (Gahtan *et al.*, 2005; Liu and Fetcho, 1999), photoliberation (Korkotian *et al.*, 2004; Park *et al.*, 2001), and the optical control of neural activity (Wang *et al.*, 2007); all take advantage of the ability to direct the laser beam to specific regions or even a single point on the specimen. In the case of spinning-disk confocals, such applications are less common or may not be feasible. Point scanners also have an optical-zoom capability, where the specimen is sampled at higher magnification by scanning a smaller region of the sample. This is also useful in, for example, laser-ablation experiments where the full laser power can be directed into a small spot at the center of a target neuron (Liu and Fetcho, 1999; O'Malley *et al.*, 2003). Ultimately, the signal generated at a point on the specimen comes down to issues of pixel-dwell time, illumination intensity and emission-collection efficiency. In effect, both instrument types are doing the same thing, but with the spinning disk many points are scanned in parallel. The key issue, for many applications, is whether or not the benefits of parallel data-collection offset the lack of an easily adjustable pinhole aperture.

### C. Dynamic Imaging with Confocal Microscopes

Researchers have used confocal microscopy to image calcium dynamics, other second messengers, protein diffusion, cell and organelle motility, cell division, and the growth of cellular processes such as neuronal axons and dendrites. Here, the speed of disk scanners is an apparent advantage, but given the fixed pinhole, photodamage, and photobleaching may become limiting because higher intensities may be needed to generate the signal necessary for dynamic tracking experiments. Conversely, when opening the pinhole aperture of point scanners, more signal is obtained (for a given intensity of illumination), but the accompanying loss of $z$-resolution may degrade the ability to follow the objects or structures of interest. While point scanners are slower to acquire full frame images, they collect smaller 2D images at physiologically relevant speeds and acquire 1D (line-scan) images very rapidly, as in some of the earliest confocal calcium imaging experiments where line-scans provided 2-ms temporal resolution and excellent 1D spatial resolution of nuclear and cytoplasmic calcium signals (Hernandez-Cruz *et al.*, 1990). This combined spatial–temporal resolution, in dynamic units of milliseconds$\times$microns-squared (discussed in O'Malley *et al.*, 2003), may not be easily attainable with spinning-disk confocals. The utility of the line-scanning approach, however, depends on being able to obtain the desired experimental result with a spatially 1D image—an outcome that is frequently achieved (see examples below).

Ultimately, the basic interaction between light and sample is the same for point-scanning and spinning-disk instruments: The laser beam dwells on a pixel for some set amount of time, photons are absorbed, and signal photons are emitted. Faster acquisition with either line-scans or spinning-disk confocals does not alter this

fundamental interaction, nor does it minimize the intrinsically damaging nature of light. If the sample is not light sensitive, the faster 2D acquisition of pixels via spinning disks is clearly advantageous. But what is generally important is the "photodose cost" per unit signal obtained, and this is a direct function of pinhole aperture. The wider the confocal aperture, the lower the photodose (illumination) needed to deliver a given quantity of signal photons to the detector. Because scanning disk pinholes are usually set to optimize optical sectioning, they reject many photons that are collected during point-scanning experiments where the pinhole aperture has been opened to some extent. Such issues notwithstanding, spinning-disk confocals have been used to image many dynamic processes such as secretory granule movements and exocytosis (Varadi *et al.*, 2002), neuronal cell death (Sun *et al.*, 2001), phagocytotic infections (Chua and Deretic, 2004), lipid signal transduction (Blazer-Yost *et al.*, 2004), cytoplasmic streaming (Serbus *et al.*, 2005), and photoreceptor calcium dynamics (Cadetti *et al.*, 2006). As documented in these varied examples, spinning-disk microscopy is useful in 3D and 4D (3D+time) applications, yet much of the fastest (millisecond resolution) cellular imaging has been accomplished via point scanning. We focus in the next section on calcium sparks—highly localized calcium responses that evolve on a millisecond time scale. These calcium sparks serve as a benchmark test of dynamic imaging performance.

Calcium sparks have been repeatedly visualized using point-scanning instruments, often in line-scan mode (see, e.g., Cheng *et al.*, 1993; Hui *et al.*, 2001; Lopez-Lopez *et al.*, 1994; Parker *et al.*, 1996; Wang *et al.*, 2001). Spinning-disk confocals have been less frequently employed, but Lothar Blatter's group has used both a Yokogawa spinning-disk instrument and a Zeiss point-scanning instrument to visualize calcium sparks (Fig. 2; from Kockskamper *et al.*, 2001). The 2D scanning disk images were collected at 17-ms intervals and were used to localize calcium release sites (Fig. 2A and B). Point-scanning confocal was then used to measure calcium events at multiple sites at 2 ms or better temporal acquisition speeds (Fig. 2C). This shows the complementary nature of these competing imaging modes. The rapid 2D imaging proved useful in visualizing the 2D distribution of calcium hot spots—which appear as a perimembrane ring. Recording of 1D line-scans, parallel to the cell's long edge, then yielded the best resolution of the hot-spots' temporal dynamics. Line-scans should be used with caution. For example, an apparent "variable amplitude" of calcium sparks can result from the scan line being offset slightly from the precise center of the calcium spark location (Pratusevich and Balke, 1996).

It should be noted that point scanners can do reasonably fast 2D imaging, as had been done earlier to visualize calcium influx rings in cultured neurons, with subsequent line-scanning used to precisely measure the flux of calcium ions across the nuclear envelope (O'Malley, 1994). The 2D images in most cases provide sufficient information to pick an appropriate location to conduct 1D line-scans (see Fig. 3 in O'Malley *et al.*, 2003). Given their longer commercial availability, point-scanning instruments have (not surprisingly) a rich history of physiological

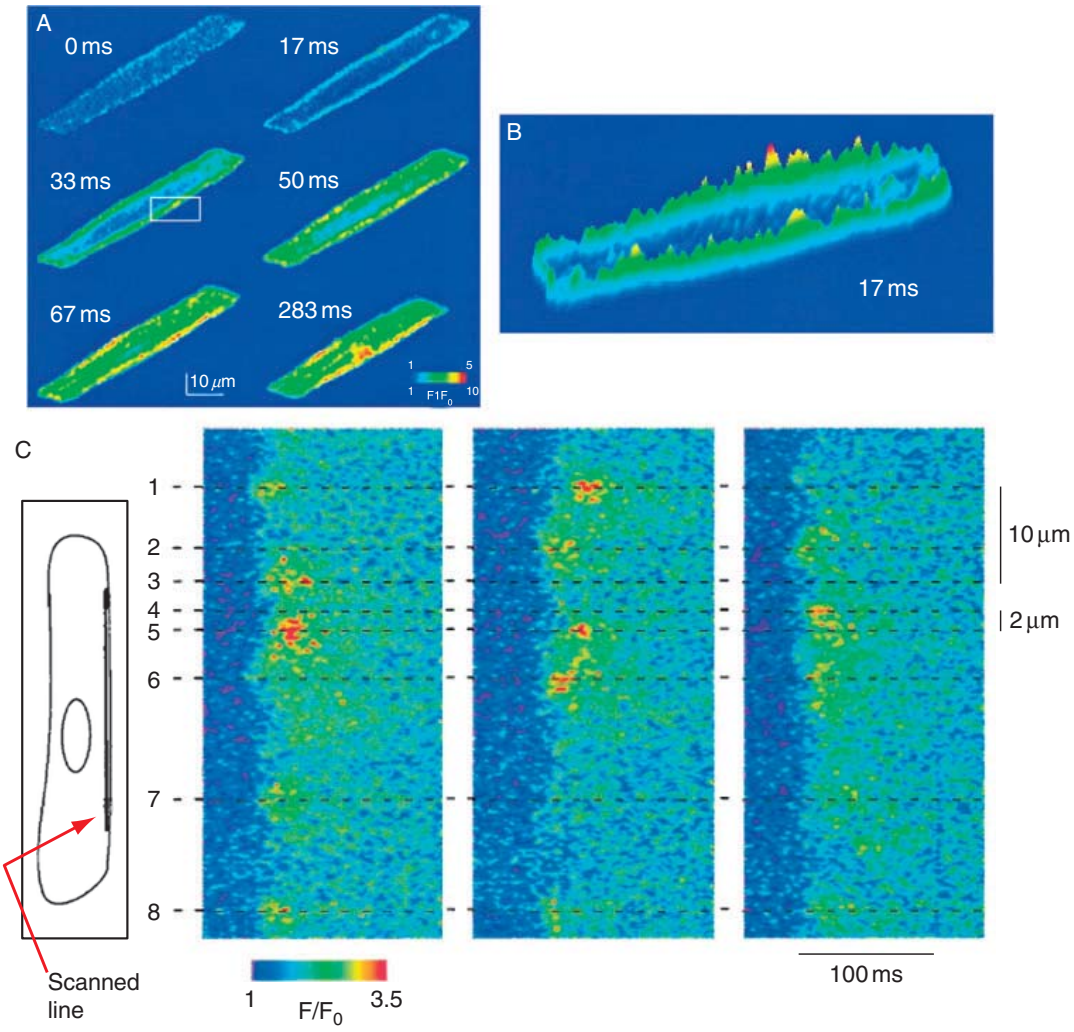


**Fig. 2** *Spinning-Disk* and *Point-Scanning* confocal images of calcium sparks in atrial myocytes. (A) Spinning-disk images acquired at 60 frames/s show a ring of calcium influx at an early moment of an atrial action potential. (B) A surface plot of the calcium image at 17 ms shows calcium peaks in the sub-sarcolemmal space. (C) Line-scans oriented along the sub-sarcolemmal space provide a more detailed record of the temporal dynamics of the calcium sparks occurring at different locations. Reprinted with permission from the *Biophysical Journal* (from Kockskamper *et al.*, 2001).

imaging results (see, e.g., Cheng *et al.*, 1993; Denk *et al.*, 1995; Fetcho and O'Malley, 1995; Fetcho *et al.*, 1998; Lipp *et al.*, 1996; Lumpkin and Hudspeth, 1995; Svoboda *et al.*, 1996, 1997; Williams *et al.*, 1994; Zhou *et al.*, 1997). But even in recent years, much of the highest temporal-resolution imaging continues to be done with point-scanning confocal and two-photon instruments (Augustine *et al.*, 2003; Gahtan *et al.*, 2002; O'Malley *et al.*, 2003, 2004; Photowala *et al.*, 2005; Scheuss *et al.*, 2006; Yasuda *et al.*, 2004). Further developments in the field include

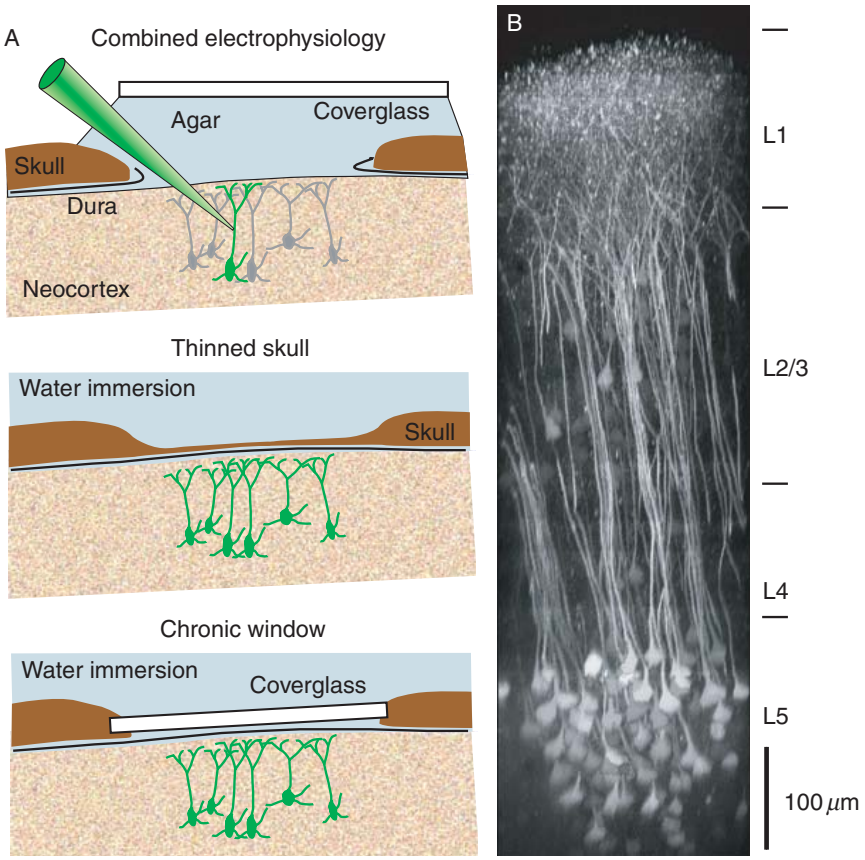


**Fig. 3** Deep tissue imaging with two-photon microscopy. Mouse neocortex is visualized with the three different methods shown in (A). Shown in (B) is a side (*xz*) view of two-photon image stack. In a transgenic mouse expressing the genetically encoded chloride indicator Clomeleon, layer 5 (L5) pyramidal cells can be visualized as much as 700 $\mu$m deep into cortex. Reprinted with permission from *Nature Methods* (from Helmchen and Denk, 2005).

"resonance scanners" that scan points more rapidly than older model point scanners (Eisenstein, 2006), and newer slit-scanning models that can sample small regions at high frequencies (Bembenek *et al.*, 2007; Gasparini *et al.*, 2007). It is not yet clear whether or not these new approaches will match or outperform traditional point- and disk-scanning confocals.

All of these confocal imaging approaches can be successful across diverse imaging applications. In regards to pushing the envelope of dynamic imaging, a prudent approach would be to critically assess the combined spatial–temporal resolution of competing instruments in published dynamic recordings. One development to track is the increasing sensitivity of electron-multiplying or EMCCD cameras (Chong *et al.*, 2004; Guntupalli *et al.*, 2005; Smith *et al.*, 2004), which may allow Nipkow-disk machines to operate at lower light intensities. Another issue is

whether or not phototoxicity and photobleaching are related in a nonlinear fashion to light dosage within some critical time window. In such a case, Nipkow disks, by briefly crossing pixels but using a high repetition rate of, for example, 250 times/s, effectively spread out the photodose over separated time epochs. Whether or not a ''greater continuous dose'' that might occur with line-scans would increase phototoxicity or photodamage has not been rigorously determined (see discussion in Donnert *et al.*, 2007b), but opening the pinhole aperture would offset this to some degree. The ultimate future of this technological competition remains uncertain, but there are several clear differences: Point scanning enables tailored laser-scan patterns, subcellular targeting, aperture-related signal increases, and optical zoom, while the scanning-disk confocal allows direct viewing of the sample and rapid acquisition of 2D, 3D, and 4D datasets.

Regarding the increasing popularity of disk scanners, this may be due in part to the perceived utility of ''seeing'' the specimen in confocal mode, but one also wonders whether purchasing decisions have been influenced by frequent claims of superior live-cell imaging capabilities, such as: ''Traditional confocal microscopes can be too slow to study the most rapid cell processes, and the intensity of laser light can damage living cells,'' (Chapman, 2003) or ''Spinning disk instruments are also optimized for live-cell imaging (and)...provide the technology for rapidly collecting images while minimizing cell damage,'' (Borg *et al.*, 2005). Certainly spinning-disk instruments can kill cells (Knight *et al.*, 2003), while point-scan-based imaging has been used to acquire intermittent calcium responses from a single nerve cell over a period of more than 24 h (Fetcho *et al.*, 1998). But the truth is that lasers used in any fashion can be used to kill cells, and as shown quantitatively by Knight *et al.* (2003), reducing laser power is the best way to minimize phototoxicity in confocal imaging. Whether or not the option of opening a pinhole aperture will benefit a given experiment depends upon the specifics of that experiment. Both style confocals offer great research opportunities, that are amplified by the ongoing revolution in genetic imaging tools, but ultimately, as it turns out, both instruments pale in comparison to a newer and even more revolutionary imaging modality: two-photon (or multi-photon) imaging.

## D. Two-Photon Imaging: Basics

At some combination of specimen thickness and specimen scattering/turbidity, all confocal imaging techniques ultimately fail. While some animals, such as zebrafish, can be made more transparent by mutagenesis or by treatment with a pigment-inhibiting compound (Elsalini and Rohr, 2003; Karlsson *et al.*, 2001; Lister *et al.*, 1999), most animals/tissues are more scattering or opaque and thus pose great obstacles if one wishes to obtain microscopic details at any significant depth. Fortunately as one shifts to longer wavelengths, in the IR range, and by using very intense pulses of light, one can take advantage of nonlinear photon absorption processes to effect a new kind of imaging: two-photon (or multi-photon) fluorescence microscopy (Denk and Svoboda, 1997; Denk *et al.*, 1990;

Piston, 2005). Using pulsed lasers, extremely high-photon fluxes can be created in a small-focal volume [with roughly the dimensions of the point-spread function (PSF) of a point object]. The result of such intense photon fluxes is that some fluorophores will be struck by two photons with sufficient simultaneity that the two photons appear, energetically, to be one higher-energy (shorter-wavelength) photon. In other words, a fluorophore that would normally absorb a single 400 nm photon can absorb two 800 nm photons—but only under extreme photon flux conditions. This seemingly esoteric phenomenon, when implemented with IR lasers, has three key consequences that make two-photon microscopy a technique of extraordinary power.

First, IR light penetrates biological tissues much more effectively than do short wavelengths (as can be seen by holding a green vs a red laser pointer against one's finger), which means that fluorophores can be effectively excited much deeper inside tissues or animals. This feature (which is complemented by the next two features), effectively opens up a new realm within which high-resolution microscopy can be performed. Secondly, and crucially, two-photon absorption occurs almost entirely within a small-focal volume, because the probability of two photons striking a fluorophore simultaneously falls off dramatically outside this volume. This means that two-photon *excitation* provides intrinsic optical sectioning. The resulting images can be similar to confocal images in circumstances suitable for confocal, but in many tissues, confocal fails with depth because one-photon absorption processes are occurring above and below the focal plane, leading to reduced contrast. This, in conjunction with scattering of both the exciting light and the return emission, can lead to total loss of contrast, despite the use of confocal pinhole apertures. The scattering of the illuminating light is less problematic for two-photon imaging, as long as the photon flux at the focal volume remains high-enough to generate two-photon excitation events. This brings us to the third consequence of this imaging modality, namely that the scatter of the *emitted* light does not significantly degrade the optical signal or image quality. Because the vast majority of emitted photons are originating from the 2P-focal volume (providing intrinsic $xy$- and $z$-resolution), it does not matter how many times photons are scattered so long as they exit the sample to reach a detector (Helmchen and Denk, 2005). For this reason, two-photon instruments are designed to collect every possible photon that leaves the sample, which improves the signal-to-noise ratio. These attributes of two-photon imaging, along with other benefits, such as the lack of photobleaching or photodamage outside the plane of focus, have led to tremendous proliferation and usage of two-photon microscopes.

When this technology first appeared, confocal microscopes were adapted to two-photon mode by switching to pulsed lasers (typically titanium-sapphire) and using the confocal laser-scanning optics to scan the pulsed-laser beam (as a diffraction-limited spot of light) across the sample. The emission was then (preferably) routed to an external detector, to avoid light losses along the confocal light path to an internal detector. One feature of two-photon is that if one takes a molecule's normal (1P) absorption spectrum and multiplies it by 2 (as a first approximation),

the spectrum becomes broader and so any given fluorophore can be excited by a broad range of wavelengths (Xu *et al*., 1996). A corollary of this broad excitation spectrum (referred to as a two-photon ''cross section'') is that one can often use a single long-wavelength source to excite multiple, different wavelength fluorophores in double- or triple-labeling experiments. Moreover, since the excitation wavelength is in the IR domain, one can, in effect, use most of the visible spectrum for collecting signal, without need for multiple barrier filters to block multiple visible excitation wavelengths. Nonlinear excitation can be extended further to three-photon excitation processes, exciting molecules in the ultraviolet bands (Xu *et al*., 1996). For this reason, one often sees the term ''multi-photon'' used instead of ''two-photon,'' but these terms refer to the same imaging systems.

## E. Two-Photon Imaging: Applications

Two-photon (point scanning) microscopes are now used in many diverse applications but are especially prevalent in neuroscience where researchers visualize morphological plasticity (Holtmaat *et al*., 2005; Knott *et al*., 2006), synaptic circuits in brain slices (Cox *et al*., 2000; Nägerl *et al*., 2004), and neuronal population activity *in vivo* (Heim *et al*., 2007; Kerr *et al*., 2005). Indeed, it is possible to resolve subcellular features down to the deepest layers of living mouse neocortex (Fig. 3; from Helmchen and Denk, 2005). In Figure 3, deep pyramidal neurons have been labeled with the genetically encoded chloride indicator clomeleon. The axons of layer 5 pyramidal cells can be seen coming off the somata as deep as 700 $\mu$m into cortex. As with confocal, two-photon is often used in line-scanning mode to maximize combined spatial–temporal resolution. It is also possible to combine two-photon absorption with Nipkow-disk scanning instruments, and this can produce better results than obtained by confocal disk scanning (Egner *et al*., 2002b). One potential drawback of disk scanning two-photon is that the laser light is distributed over many points, possibly making it less suitable for deep tissue imaging than point-scanning two-photon. While this issue does not yet seem to have been experimentally addressed, the depth of useful imaging is clearly related to the amount of laser power that can be transmitted (and focused) to the desired imaging depth (Helmchen and Denk, 2005).

In terms of imaging trade-offs between confocal and two-photon imaging, it seems that two-photon systems either ''tie'' or ''win'' across the board in such terms as signal-to-noise, resolution, decreased photobleaching, depth of penetration, and localization of optical manipulation (as in laser-ablation, photoactivation, or optical control of membrane potential). In theory, confocal should have a spatial-resolution advantage because of its shorter-wavelength of illumination. But in practice, it seems that this starting advantage is rapidly lost, presumably because of out-of-plane absorption and scattering of both the exciting and emitted light. This does not mean that one should not try confocal. Figures 4 and 5 show, respectively, confocal and two-photon images (maximum projections) of the zebrafish brainstem (from two different zebrafish larvae) in which large numbers of

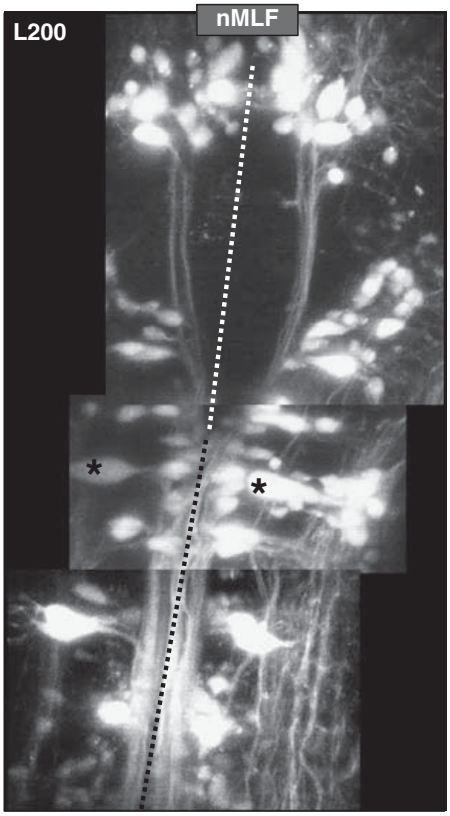


**Fig. 4** Confocal montage (of maximum projections) of reticulospinal neurons in the brainstem of a restrained larval zebrafish. Neurons were labeled using the labeled-lesion technique in which large numbers of neurons are simultaneously labeled with fluorescent dextrans and disconnected from their spinal targets (Gahtan and O'Malley, 2001). Such lesions result in novel and highly abnormal bending patterns due to deconstraint of the spinal neural circuits (Day *et al*., 2005). Image courtesy of Leslie Day, Department of Biology, Northeastern University.

reticulospinal neurons were retrogradely labeled by injecting a fluorescent tracer into spinal cord. Both images show many details of neuronal cell bodies, axons, and dendrites that would not be evident if using wide-field fluorescence microscopy, even if deconvolution techniques were employed (see below). This is not a rigorous comparison because the specimen is not stable enough for perfectly equivalent image acquisition on two remote platforms, but our impression from looking at many such confocal image stacks is that finer structural details (at depths 200 $\mu$m or deeper into the larval brain) are evident in the two-photon image.

With two-photon, one can readily perform all of the techniques associated with point-scanning confocal including laser-ablation, FRAP, and photo-uncaging. In conjunction with a rapid 2D acoustical-optical device, single-point, two-photon imaging is able to rapidly image neural activity at sparsely distributed sites (Iyer *et al*., 2006). The most serious drawback to two-photon is its cost, which is equal to the cost of a high-quality confocal system plus an additional $100,000 or

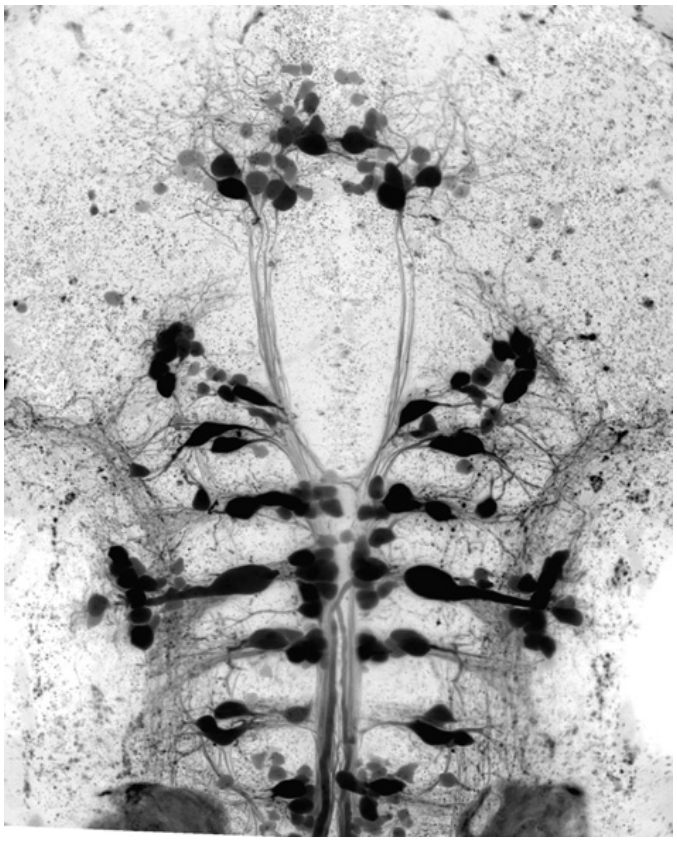

**Fig. 5** Two-photon projection of reticulospinal neurons in the brainstem of a restrained larval zebrafish. Neurons were labeled with Texas-red dextran (10,000 MW) and slow-scan imaged with a 20X, 0.95 NA objective to produce maximum resolution deep inside this living animal. Contrast has been reversed (the darkest cells are the most fluorescent). Fine anatomical details (of e.g., axons and dendrites) are evident that are difficult to resolve in confocal images of similarly labeled fish. Image courtesy of Michael Orger, Adam Kampff, J. H. Bollmann and Florian Engert, Department of Molecular Cellular Biology, Harvard University.

so for the pulsed laser (although a number of enterprising labs have built such systems on their own; Majewska *et al.*, 2000). Two-photon systems are also trickier to maintain and operate, but commercial vendors are working to make these systems more turnkey and user friendly. This does not mean that everyone needs to or should buy a two-photon system: If the less expensive microscopes described here achieve your experimental goals, the money saved can be spent elsewhere.

## F. Deconvolution

Deconvolution represents yet another dimension of biological imaging, within the "image analysis" domain. The term "deconvolution" refers to a variety of image improvement techniques that mathematically "deblur" or otherwise "restore"

microscopic images acquired by various imaging modalities. There are a number of detailed reviews of the different variations of these methods (see, e.g., McNally *et al.*, 1999; Sarder and Nehorai, 2006; Wallace *et al.*, 2001). In contrast to confocal and two-photon, which use optical tricks to optimize the resolution of objects (by minimizing the size of the diffracted, microscopically recorded image), deconvolution uses algorithms to undo this diffraction, that is to undo the optical PSF of the object. In principle, deconvolution is agnostic with regard to the imaging modality used to acquire an image, but ultimately, as with the imaging modalities themselves, its performance is dependent upon signal-to-noise issues. Deconvolution can be applied to 2D images (see, e.g., Donnert *et al.*, 2007a), but is more commonly applied to 3D data sets, including those acquired by conventional fluorescence microscopes with a motorized objective. Some proponents have argued that deconvolution offers a cheaper and potentially superior alternative to confocal microscopy, to the point of one manufacturer labeling a deconvolution control on a wide-field fluorescence microscope as "confocal." In order to deblur this encroachment between optical and mathematical techniques, we will consider several applications of deconvolution including its use with confocal and two-photon microscopes.

3D-deconvolution seeks, in effect, to maximally undo the physical, *z*-axis spread of light from an optical point source. This diffraction-based spread of emitted light normally makes *z*-axis resolution about threefold worse than *xy*-plane resolution and so one goal of deconvolution is to whittle this diffracted image down to a representation more closely resembling its true 3D physical size. Figure 6A and B (from Schrader *et al.*, 1996) show the effect of deconvolving already fine confocal point-spread functions (namely images of 50 nm gold beads mounted in immersion oil). The remarkable degree of "resolution" obtained for both the confocal and deconvolved images are discussed in more detail in Section IV, but the principle result from this example, using a maximum-likelihood estimation deconvolution algorithm (that is well suited for the restoration of photon-limited images), is a reduction in the *xy*-plane's PSF from 80 nm down to 40 nm, and a reduction in the *z*-plane's PSF from 460 nm down to 145 nm. This impressive result was obtained under stringent conditions (described below) and as such provides an upper bound on the degree of resolution that might be achieved under optimal circumstances. This particular result is unlikely to be achieved with most experimental preparations, or with wide-field fluorescence microscopy, but deconvolution can, under favorable circumstances, improve many biological images and yield data that is more readily interpreted.

So what can deconvolution really do? This approach works best with relatively non-scattering samples and is degraded with increasing depth into scattering samples. Once one ventures deeper into living specimens, the waters often become murky. There are clear instances where deconvolution results in better image quality, and this can be true in both wide-field (conventional) fluorescence microscopy (Falk and Lauf, 2001; Ferko *et al.*, 2006; Jang and Ye, 2007; Manz *et al.*, 2000) and with confocal image stacks (Difato *et al.*, 2004; Strohmaier *et al.*, 2000). Yet there are other reports indicating that deconvolution adds minimally to

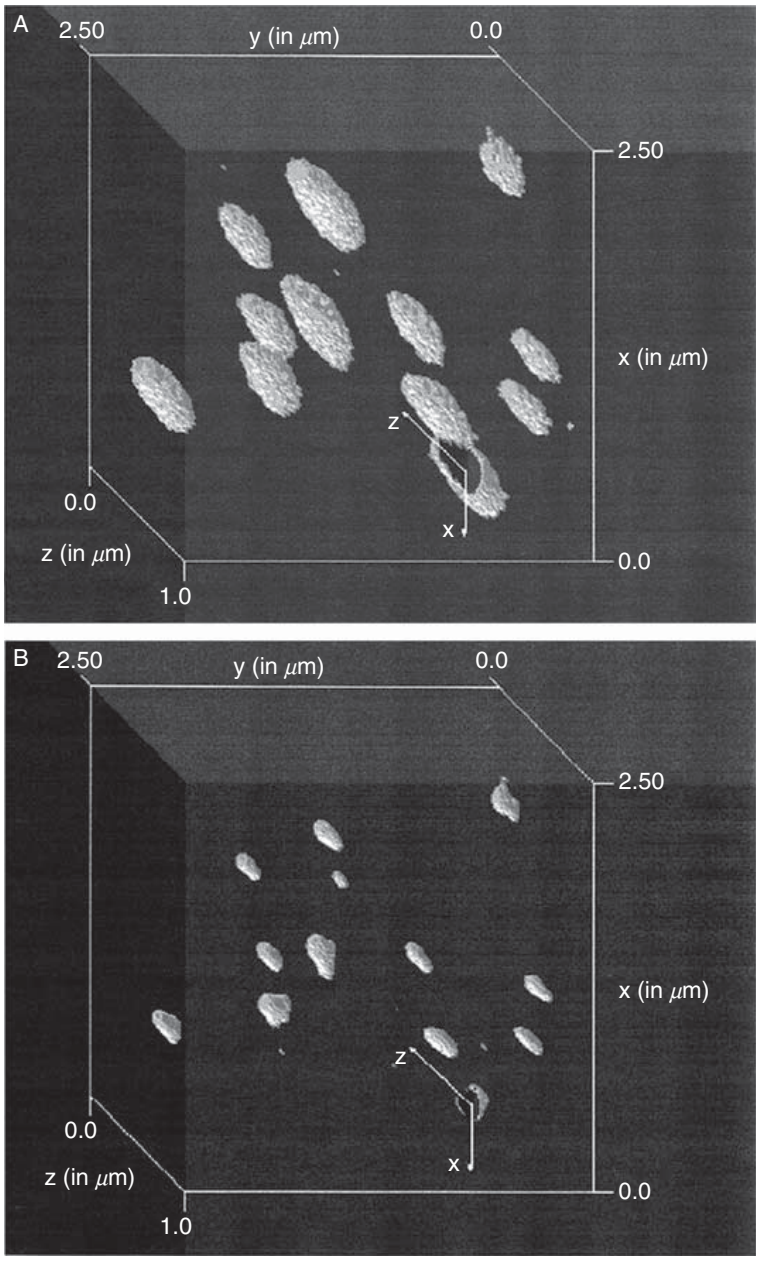


**Fig. 6** Deconvolution of confocal image stack. Gold beads (50 nm) were dispersed in immersion oil and imaged using a 3D-piezoelectric stage-scanning confocal microscope. 3D stacks consisted of 30 *xy* images that were 40 nm apart in the *z*-direction. The pixel size was 10 nm in the *xy* plane. (A) Shows a rendered plot of the bead images. The beads are less than one-seventh of the illumination wavelength and so their rendered confocal images represent, in effect, the optical point-spread function. (B) Use of a maximum-likelihood deconvolution algorithm restores the images to a more faithful representation of the actual object dimensions. Reprinted with permission from *Applied Physical Letters* (from Schrader *et al.*, 1996).

confocal imaging (Wako *et al.*, 1998) and that it does not perform well with certain far-field image specimens (Verveer *et al.*, 1999). In any case, it is straightforward to apply deconvolution algorithms to 3D datasets, and so it makes sense to try. Deblurring "freeware" is available from several sources (Majewska *et al.*, 2000), including NIH Image (or ImageJ for PC computers), while a variety of more extensive packages are available from commercial vendors.

Note that any image stack can be subjected to 3D deconvolution algorithms, but for this to be meaningful there must be shared optical information between neighboring images in the *z*-stack (i.e., overlapping PSFs in the *z*-dimension). If the image planes are much further apart, 3D deconvolution will not achieve much. Assuming the datasets are suitable, the different deblurring and image reconstruction techniques should generally provide some image improvement, but there are a variety of artifacts that may frequently appear (Majewska *et al.*, 2000; McNally *et al.*, 1999), and so it is important to (1) optimize image acquisition parameters/conditions and (2) ensure that for any "structures" revealed in the deconvolution process, there is at least some evidence of those structures in the raw images.

The most controversial point encountered in this literature is whether or not deconvolution can replace or even exceed the performance of confocal imaging (see, e.g., Verveer *et al.*, 2007). Maierhofer *et al.* (2003) suggest that confocal has worse signal/noise than far-field deconvolution approaches and is more seriously affected by photobleaching, but no comparative confocal data are provided. Their report does provide elegant multicolor deconvoluted image stacks of clinical tissue samples, revealing details important for analyzing cytogenetic defects, but given that these are 30-$\mu$m thick, paraffin embedded, dehydrated specimens, this sample does not provide the optical challenge of many specimens, in terms of depth or light scattering. In certain instances, a combination of wide-field fluorescence imaging and deconvolution might be preferred over confocal. For example, in voltage-imaging studies in the relatively translucent olfactory bulb of the salamander, the voltage–dye signals are limited in quantity and durability and any photons lost by confocal optical sectioning would adversely affect signal-to-noise ratios (Cinelli, 2000). In this case, deconvolution of wide-field images helps to assign voltage signals to the appropriate regions and layers of the olfactory bulb in which the neural activity is occurring. Indeed, the tissue is optically segmented into 20-$\mu$m sections and the deeper depth-of-field of conventional fluorescence optics delivers more signals, yielding images that can be subsequently improved by deconvolution. The nature of this strategy is analogous to opening the pinhole of point-scanning confocal microscopes: If it is useful to integrate signal from (for example) a whole nerve cell body, then an open aperture will collect more of the cell's emission, improving the signal-to-noise ratio.

Still, in many applications, confocal is able to extract signals that are simply lost in the blur of wide-field fluorescence imaging. A cell visualization chapter in a popular cell and molecular biology textbook has a particularly nice example of this, while providing related deconvolution results (Alberts *et al.*, 2002). This is not to say that deconvolution is not valuable, but rather that one should acquire data

with the best tools available and then judiciously employ different deblurring and restoration algorithms to see if the data can be meaningfully enhanced. While the rank order of depth of penetration (with good resolution) is clearly two-photon > confocal > wide-field deconvolution, the rank order of availability/economy is clearly deconvolution > confocal > two-photon. This is another example of the trade-offs encountered in imaging, but this one concerns economics rather than biophysical constraints.

## G. CCD Versus PMT

Another twist in considering competing technologies is the detector that is used in acquiring the image. While a variety of optical detectors are available, including film, your eyes, CMOS devices, vidicon cameras, and avalanche photodiodes (APDs), the most common detectors used in light-microscopic applications are CCDs (charge-coupled devices; see Aikens *et al*., 1989) and PMTs. The CCD (including its newer EMCCD or electron-multiplying version) is in widespread use in diverse applications including consumer digital cameras, and is now the most common detector for both basic fluorescence microscopes and spinning-disk confocals. In contrast, PMTs (and sometimes APDs) are used in point-scanning confocals and two-photon instruments. As with the different modes of imaging, each detection mode has its own specific strengths and limitations.

Typically, the first question will be ''which detector is more sensitive?'' Sensitivity is poorly defined and even more difficult to compare, given the problem of comparing identical, appropriate samples on different platforms in a fair and meaningful way. One is left with the claim that ''CCDs are more sensitive than PMTs'' because they have higher quantum efficiency (the efficiency with which each impinging photon is converted into a photoelectron). It is true that CCDs can have quantum efficiencies of 90% or higher, while PMTs have efficiencies less than 10%, which might make CCDs seem the obvious choice. But what this simplified comparison lacks is consideration of the signal that is ultimately delivered by the imaging device. Each pixel in the CCD is read out serially and when reading out small signals very quickly (which is necessary for dynamic imaging applications that require rapid pixel read-out rates), one encounters as much as 20 electrons worth of read-out noise (James Pawley, confocal listserv, 10/6/07, http://listserv.buffalo.edu)—which makes it difficult to use signals on the order of 10 or 15 photons per pixel (with each detected photon producing a single photoelectron). In contrast, the PMT amplifies each photon that it does convert into an electron by up to a millionfold (depending on amplifier gain). If the PMT receives 20 photons, it will detect only about 10% of these (one or two photons), but for each photon detected it will amplify the signal enormously, with minimal read-out noise.

Given the foregoing considerations, the true disparity in performance is not so great as to dictate which type of instrument (spinning disk, slit scanner, or point scanner) to choose: Each detector serves its host microscopes well. The newest

generation EMCCD (electron-multiplying CCD) detectors have greater sensitivity due to their incorporation of an amplification step prior to the read-out stage (Chong *et al.*, 2004; Guntupalli *et al.*, 2005; Smith *et al.*, 2004), which may improve the dynamic imaging abilities of disk- and slit-scanning confocal microscopes. Signal-to-noise issues take on greater importance when one is seeking to obtain finer spectral information from each pixel (sometimes referred to as ''hyperspectral'' imaging), because the photoelectrons generated from a given location are subdivided into spectral bins. Current generation CCD cameras are indeed being used for such applications, but when imaging at high speed with live samples, one must consider the sample's sensitivity. To achieve high-enough emission fluxes to fill all of the ''imaging wells'' (the spectral split of signal from each pixel location) and produce signal in excess of the noise, one must consider, as James Pawley has put it that ''phototoxicity is proportional to EXCITATIONS rather than to incident light, (and so) the emission of this much signal is likely to be unpleasant to the cell.''

## IV. Discussion: Terms of Resolution

### A. What is NOT Resolution

Resolution means resolving discrete items. This could mean *xy* spatial resolution, which is diffraction limited on conventional optical microscopes. This also applies to *z*-resolution and temporal resolution and is mentioned because of liberties that have been taken with the word. In some papers, the selected size for the *z*-axis motor-step is (quite naively) stated to be the *z*-axis resolution. While one indeed needs to make fine motor steps to if one is to produce a detailed 3D reconstruction of a specimen, the *z*-axis PSF and the motor step size are wholly unrelated entities. More common are claims that the acquisition speed of a device is the temporal resolution, with for example claims that events 2-ms apart can be resolved by 2-ms line-scans. This is equally invalid because one may need to bin together multiple pixels in time if one is to resolve, that is distinguish, discrete events separated in time. Whether discussing calcium dynamics (as above), or other cellular events, temporal resolution (like spatial resolution) depends on BOTH the imaging system's performance (microscope, detector) AND the signal-to-noise ratio of the pixels being acquired. One can often improve temporal resolution by spatially binning together pixels (i.e., trading off spatial resolution) or conversely, bin pixels over time to better resolve the spatial aspects of dynamic events, but like Heisenberg's uncertainty principle, you cannot do both at the same time. In the case of calcium dynamics, there is asymmetric resolution in time: with 2-ms line-scans (and a little 1D spatial binning), it is possible to reliably detect step (2 ms) increases in fluorescence, but closely following subsequent events may not be easily resolved or even detected because of the slow recovery dynamics of calcium signals. In this instance, the resolution is not compromised by pixel noise, but rather by the dynamics of the biological events themselves.

### B. What IS Resolution—Resolution from Hell

Stefan Hell and colleagues (Schrader *et al.*, 1996) present optical limits that one can obtain with confocal microscopy, achieving Full Width Half Maximum (FWHM) values of 460 nm in the *z*-dimension and 145 nm in the *xy*-plane (Fig. 6A; sample was illuminated with a 543 nm helium–neon laser). With deconvolution (maximum-likelihood method), these FWHM values are reduced to 80 nm (*z*) and 40 nm (*xy*) (Fig. 6B). The FWHM value is not *resolution* per se, but two-point objects that are separated by the FWHM distance would be distinguishable as discrete objects, that is, resolved. How is such remarkable resolution obtained? This result depended upon a set of conditions namely: (1) use of high-contrast 50 nm gold beads as targets, (2) slow scanning to optimize the signal/noise ratio, (3) placing the beads in immersion oil to avoid refractive-index mismatch-induced spherical aberration, and (4) use of a 3D piezoelectric stage-scanning microscope. Few labs have this specialized type of microscope, although piezoelectric controlled stages are seeing increased use. Moreover, oil-immersed gold beads are not representative of many biological samples, nor is the 10-$\mu$m thickness of the sample terribly ''deep'' in the context of our current discussion. But this does illustrate, in dramatic fashion, the potential resolution that one can obtain inside an actual 3D structure, with conventional light-microscopic imaging, given certain necessary conditions (instrument-wise and sample-wise) and the application of image restoration techniques. Given the ongoing advances in both instrumentation and super-resolution techniques such as STED and STORM (Hell, 2007; Rust *et al.*, 2006), our resolution of living biological structures and dynamic events may extend into entirely new domains.

### C. Whole-Animal Imaging

At the largest spatial scale, one can look deep into the interior of animals using visible, positron, X-ray, and radiofrequency radiation, as well as using sound waves. In the ''human brain mapping'' genre, neural activation patterns are revealed using positron emission tomography (PET) or functional magnetic resonance imaging (fMRI), but these approaches cannot detect individual neurons or axons. Instead they provide a regional, aggregate signal based on neural activation of volumes of brain tissue that may consist of tens or hundreds of thousands of cells. A number of techniques are being used to try and bridge the gap between regional brain mapping techniques and cellular–subcellular level imaging approaches. Techniques involving novel labeling approaches, transgenic animals and *in vivo* two-photon imaging are all beginning to reveal circuit-level details (Feng *et al.*, 2000; Fetcho and O'Malley, 1997; Gahtan and O'Malley, 2003; Gahtan *et al.*, 2002; Göbel *et al.*, 2007; Kerr *et al.*, 2005; Orger *et al.*, 2008; Stosiek *et al.*, 2003). Other *in vivo* techniques, such as bioluminescent imaging, can reveal distribution patterns of cell populations in intact mice, and have been used, for example, to track tumor metastasis as well as the proliferation and movements of tumor killing cells (see, e.g., Dickson *et al.*, 2007;

Edinger *et al.*, 2003; Jenkins *et al.*, 2005; Wetterwald *et al.*, 2002). While such techniques are not able to resolve individual tumor cells or other fine tumor structure (Bhaumik and Gambhir, 2002; Deroose *et al.*, 2007; Kuo *et al.*, 2007; Shcherbo *et al.*, 2007; Weissleder and Ntziachristos, 2003), they do provide a noninvasive means to track and quantify tumor burden and distribution and evaluate efficacy of therapeutic compounds in different animal models of cancer. What we still cannot do is perform cellular- and subcellular-resolution imaging and optical manipulation deep in the tissues of mammals to either investigate neural circuitry or study pathological processes like cancer. This will have to await future technological breakthroughs.

## V. Summary

Biologists would like to visualize molecular-scale processes deep inside animals (including humans) and would like to do so with good specificity and spatial–temporal resolution. There are formidable barriers to this goal, but the diverse approaches reviewed, and the ingenuity with which increasingly powerful techniques are being created, suggest that the great advances of the past 20 years could be matched over the next 20 years. Such advances would become increasingly important for both the natural scientist and the clinician. To look deep into a diseased human body and record molecular events with great specificity, precision and context would provide a treasure trove of information. This would allow us to examine complex physiological and pathological processes from a Systems Biology perspective. But for the present we cannot—we immediately encounter trade-offs even in our more depth- and specimen-limited imaging efforts. Biological imaging today is about trade-offs: trading off spatial resolution for either depth of imaging or speed of acquisition, and trading off temporal resolution to see structures in finer detail. Judicious choosing of technologies, in conjunction with a great variety of new molecular probes, will best allow researchers to negotiate the pertinent trade-offs and work towards visualizing cells, tissues, and organisms in their full 3D splendor.

### Acknowledgments

The author appreciates comments from Barry Burbach, as well as extensive and generous help from many members of the confocal newsgroup, whose public list archives can be accessed via http://listserv.buffalo.edu.

### References

Ackerley, C. A., Nielsen, C., and Hawkins, C. E. (2006). Experiences with wet capsule imaging exploring the potential for live cell imaging. *Microsc. Microanal.* **12**(Supp 2), 428–429.

Aikens, R. S., Agard, D. A., and Sedat, J. W. (1989). Solid-state imagers for microscopy. *Methods Cell Biol.* **29,** 291–313.

Alberts, B., Johnson, A., Lewis, J., Raff, M., Roberts, K., and Walter, P. (2002). Visualizing cells. *In* Molecular Biology of the Cell. pp. 547–580. Garland Science, New York.

Amos, W. B., Reichelt, S., Cattermole, D. M., and Laufer, J. (2003). Re-evaluation of differential phase contrast (DPC) in a scanning laser microscope using a split detector as an alternative to differential interference contrast (DIC) optics. *J. Microsc.* **210,** 166–175.

Amos, W. B., and White, J. G. (2003). How the confocal laser scanning microscope entered biological research. *Biol. Cell* **95,** 335–342.

Ando, T., Uchihashi, T., Kodera, N., Yamamoto, D., Taniguchi, M., Miyagi, A., and Yamashita, H. (2007). High-speed atomic force microscopy for observing dynamic biomolecular processes. *J. Mol. Recognit.* **20,** 448–458.

Augustine, G. J., Santamaria, F., and Tanaka, K. (2003). Local calcium signaling in neurons. *Neuron* **40,** 331–346.

Axelrod, D. (2003). Total internal reflection fluorescence microscopy in cell biology. *Methods Enzymol.* **361,** 1–33.

Bagnall, M. W., Stevens, R. J., and du Lac, S. (2007). Transgenic mouse lines subdivide medial vestibular nucleus neurons into discrete, neurochemically distinct populations. *J. Neurosci.* **27,** 2318–2330.

Bancroft, J. D., and Gamble, M. (2001). Theory and Practice of Histological Techniques 5th edn. Churchill Livingston, NY.

Beis, D., and Stainier, D. Y. (2006). *In vivo* cell biology: Following the zebrafish trend. *Trends Cell Biol.* **16,** 105–112.

Bembenek, J. N., Richie, C. T., Squirrell, J. M., Campbell, J. M., Eliceiri, K. W., Poteryaev, D., Spang, A., Golden, A., and White, J. G. (2007). Cortical granule exocytosis in *C. elegans* is regulated by cell cycle components including separase. *Development* **134,** 3837–3848.

Bhaumik, S., and Gambhir, S. S. (2002). Optical imaging of *Renilla luciferase* reporter gene expression in living mice. *Proc. Natl. Acad. Sci. USA* **99,** 377–382.

Blazer-Yost, B. L., Vahle, J. C., Byars, J. M., and Bacallao, R. L. (2004). Real-time three-dimensional imaging of lipid signal transduction: Apical membrane insertion of epithelial Na(+) channels. *Am. J. Physiol. Cell. Physiol.* **287,** C1569–C1576.

Borg, T. K., Stewart, J. A., Jr., and Sutton, M. A. (2005). Imaging the cardiovascular system: Seeing is believing. *Microsc. Microanal.* **11,** 189–199.

Bos, M. A., and Kleijn, J. M. (1995). Determination of the orientation distribution of adsorbed fluorophores using TIRF. II. Measurements on porphyrin and cytochrome c. *Biophys. J.* **68,** 2573–2579.

Braeckmans, K., Remaut, K., Vandenbroucke, R. E., Lucas, B., De Smedt, S. C., and Demeester, J. (2007). Line FRAP with the confocal laser scanning microscope for diffusion measurements in small regions of 3-D samples. *Biophys. J.* **92,** 2172–2183.

Brakenhoff, G. J. (1979). Imaging modes in confocal scanning light microscopy. *J. Microsc.* **117,** 232–242.

Brakenhoff, G. J., van der Voort, H. T., van Spronsen, E. A., Linnemans, W. A., and Nanninga, N. (1985). Three-dimensional chromatin distribution in neuroblastoma nuclei shown by confocal scanning laser microscopy. *Nature* **317,** 748–749.

Cadetti, L., Bryson, E. J., Ciccone, C. A., Rabl, K., and Thoreson, W. B. (2006). Calcium-induced calcium release in rod photoreceptor terminals boosts synaptic transmission during maintained depolarization. *Eur. J. Neurosci.* **23,** 2983–2990.

Chapman, T. (2003). Seeing is believing (technology feature). *Nature* **425,** 867–873.

Cheng, H., Lederer, W. J., and Cannell, M. B. (1993). Calcium sparks: Elementary events underlying excitation contraction coupling in heart muscle. *Science* **262,** 740–744.

Chong, F. K., Coates, C. G., Denvir, D. J., McHale, N. G., Thornbury, K. D., and Hollywood, M. A. (2004). Optimization of spinning disk confocal microscopy: Synchronization with the ultra-sensitive EMCCD. *Proc. SPIE* **5324,** 65–76.

Chua, J., and Deretic, V. (2004). Mycobacterium tuberculosis reprograms waves of phosphatidylinositol 3-phosphate on phagosomal organelles. *J. Biol. Chem.* **279,** 36982–36992.

Chudakov, D. M., Chepurnykh, T. V., Belousov, V. V., Lukyanov, S., and Lukyanov, K. A. (2006). Fast and precise protein tracking using repeated reversible photoactivation. *Traffic* **7,** 1304–1310.

Cinelli, A. R. (2000). High-definition mapping of neural activity using voltage-sensitive dyes. *Methods* **21,** 349–372.

Cody, S. H., Xiang, S. D., Layton, M. J., Handman, E., Lam, M. H., Layton, J. E., Nice, E. C., and Heath, J. K. (2005). A simple method allowing DIC imaging in conjunction with confocal microscopy. *J. Microsc.* **217,** 265–274.

Collier, T., Guillaud, M., Follen, M., Malpica, A., and Richards-Kortum, R. (2007)).Real-time reflectance confocal microscopy: Comparison of two-dimensional images and three-dimensional image stacks for detection of cervical precancer. *J. Biomed. Opt.* **12:051901,** 1–10.

Concha, M. L., and Adams, R. J. (1998). Oriented cell divisions and cellular morphogenesis in the zebrafish gastrula and neurula: A time-lapse analysis. *Development* **125,** 983–994.

Cox, C. L., Denk, W., Tank, D. W., and Svoboda, K. (2000). Action potentials reliably invade axonal arbors of rat neocortical neurons. *Proc. Natl. Acad. Sci. USA* **97,** 9724–9728.

Cox, G. (2007). Optical Techniques in Cell Biology. Taylor & Francis Group, Boca Raton, FL.

Cubitt, A. B., Heim, R., Adams, S. R., Boyd, A. E., Gross, L. A., and Tsien, R. Y. (1995). Understanding, improving and using green fluorescent proteins. *Trends Biochem. Sci.* **20,** 448–455.

Dahm, R., Schonthaler, H. B., Soehn, A. S., van Marle, J., and Vrensen, G. F. (2007). Development and adult morphology of the eye lens in the zebrafish. *Exp. Eye Res.* **85,** 74–89.

Day, L. J., Knudsen, D. P., Dhanota, H., Severi, K., Jose, J. V., and O'Malley, D. M. (2005). Lesions of descending motor pathways deconstrain spinal activity patterns: Results from larval zebrafish. *Soc. Neurosci. Abs*. **31,** 751.11.

Denk, W., Holt, J. R., Shepherd, G. M., and Corey, D. P. (1995). Calcium imaging of single stereocilia in hair cells: Localization of transduction channels at both ends of tip links. *Neuron* **15,** 1311–1321.

Denk, W., Strickler, J. H., and Webb, W. W. (1990). Two-photon laser scanning fluorescence microscopy. *Science* **248,** 73–76.

Denk, W., and Svoboda, K. (1997). Photon upmanship: Why multiphoton imaging is more than a gimmick. *Neuron* **18,** 351–357.

Deroose, C. M., De, A., Loening, A. M., Chow, P. L., Ray, P., Chatziioannou, A. F., and Gambhir, S. S. (2007). Multimodality imaging of tumor xenografts and metastases in mice with combined small-animal PET, small-animal CT, and bioluminescence imaging. *J. Nucl. Med.* **48,** 295–303.

Detrich, H. W., III, Zon, L. I., and Westerfield, M. (2004). The zebrafish: Cellular and developmental biology. *Methods Cell Biol.* **76,** 1–656.

Dickinson, M. E., Bearman, G., Tille, S., Lansford, R., and Fraser, S. E. (2001). Multi-spectral imaging and linear unmixing add a whole new dimension to laser scanning fluorescence microscopy. *Biotechniques* **31,** 1274–1278.

Dickson, P. V., Hamner, B., Ng, C. Y., Hall, M. M., Zhou, J., Hargrove, P. W., McCarville, M. B., and Davidoff, A. M. (2007). *In vivo* bioluminescence imaging for early detection and monitoring of disease progression in a murine model of neuroblastoma. *J. Pediatr. Surg.* **42,** 1172–1179.

Difato, F., Mazzone, F., Scaglione, S., Fato, M., Beltrame, F., Kubínová, L., Janácek, J., Ramoino, P., Vicidomini, G., and Diaspro, A. (2004). Improvement in volume estimation from confocal sections after image deconvolution. *Microsc. Res. Tech.* **64,** 151–155.

Dodt, H. U., and Zieglgansberger, W. (1990). Visualizing unstained neurons in living brain slices by infrared DIC-videomicroscopy. *Brain Res.* **537,** 333–336.

Donnert, G., Eggeling, C., and Hell, S. W. (2007). Major signal increase in fluorescence microscopy through dark-state relaxation. *Nat. Methods* **4,** 81–86.

Donnert, G., Keller, J., Wurm, C. A., Rizzoli, S. O., Westphal, V., Schonle, A., Jahn, R., Jakobs, S., Eggeling, C., and Hell, S. W. (2007a). Two-color far-field fluorescence nanoscopy. *Biophys. J.* **92,** L67–L69.

Dwyer, P. J., DiMarzio, C. A., Zavislan, J. M., Fox, W. J., and Rajadhyaksha, M. (2006). Confocal reflectance theta line scanning microscope for imaging human skin *in vivo*. *Opt. Lett.* **31,** 942–944.

Edinger, M., Cao, Y. A., Verneris, M. R., Bachmann, M. H., Contag, C. H., and Negrin, R. S. (2003). Revealing lymphoma growth and the efficacy of immune cell therapies using in vivo bioluminescence imaging. *Blood* **101,** 640–648.

Eisenstein, M. (2006). Something to see (technology feature). *Nature* **443,** 1017–1023.

Elsalini, O. A., and Rohr, K. B. (2003). Phenylthiourea disrupts thyroid function in developing zebrafish. *Dev. Genes Evol.* **212,** 593–598.

Egner, A., Andresen, V., and Hell, S. W. (2002b). Comparison of the axial resolution of practical Nipkow-disk confocal fluorescence microscopy with that of multifocal multiphoton microscopy: Theory and experiment. *J. Microsc.* **206,** 24–32.

Egner, A., Jakobs, S., and Hell, S. W. (2002a). Fast 100-nm resolution three-dimensional microscope reveals structural plasticity of mitochondria in live yeast. *Proc. Natl. Acad. Sci. USA* **99,** 3370–3375.

Falk, M. M., and Lauf, U. (2001). High resolution, fluorescence deconvolution microscopy and tagging with the autofluorescent tracers CFP, GFP, and YFP to study the structural composition of gap junctions in living cells. *Microsc. Res. Tech.* **52,** 251–262.

Feng, G., Mellor, R. H., Bernstein, M., Keller-Peck, C., Nguyen, Q. T., Wallace, M., Nerbonne, J. M., Lichtman, J. W., and Sanes, J. R. (2000). Imaging neuronal subsets in transgenic mice expressing multiple spectral variants of GFP. *Neuron* **28,** 41–51.

Ferko, M. C., Bhatnagar, A., Garcia, M. B., and Butler, P. J. (2007). Finite-element stress analysis of a multi-component model of sheared and focally-adhered endothelial cells. *Ann. Biomed. Eng.* **35,** 208–223.

Ferko, M. C., Patterson, B. W., and Butler, P. J. (2006). High-resolution solid modeling of biological samples imaged with 3D fluorescence microscopy. *Microsc. Res. Tech.* **69,** 648–655.

Fetcho, J. R., Cox, K., and O'Malley, D. M. (1998). Monitoring activity in neuronal populations with single-cell resolution in a behaving vertebrate. *Histochem. J.* **30,** 153–167.

Fetcho, J. R., and O'Malley, D. M. (1995). Visualization of active neural circuitry in the spinal cord of intact zebrafish. *J. Neurophysiol.* **73,** 399–406.

Fetcho, J. R., and O'Malley, D. M. (1997). Imaging neuronal networks in behaving animals. *Curr. Opin. Neurobiol.* **7,** 832–838.

Frangakis, A. S., and Förster, F. (2004). Computational exploration of structural information from cryo-electron tomograms. *Curr. Opin. Struct. Biol.* **14,** 325–331.

Frankel, D. J., Pfeiffer, J. R., Surviladze, Z., Johnson, A. E., Oliver, J. M., Wilson, B. S., and Burns, A. R. (2006). Revealing the topography of cellular membrane domains by combined atomic force microscopy/fluorescence imaging. *Biophys. J.* **90,** 2404–2413.

Gahtan, E., and Baier, H. (2004). Of lasers, mutants, and see-through brains: Functional neuroanatomy in zebrafish. *J. Neurobiol.* **59,** 147–161.

Gahtan, E., and O'Malley, D. M. (2001). Rapid lesioning of large numbers of identified vertebrate neurons: Applications in zebrafish. *J. Neurosci. Methods* **108,** 97–110.

Gahtan, E., and O'Malley, D. M. (2003). Visually-guided injection of identified reticulospinal neurons in zebra fish: A survey of spinal arborization patterns. *J. Comp. Neurol.* **459,** 186–200.

Gahtan, E., Sankrithi, N., Campos, J. B., and O'Malley, D. M. (2002). Evidence for a widespread brainstem escape network in larval zebrafish. *J. Neurophysiol.* **87,** 608–614.

Gahtan, E., Tanger, P., and Baier, H. (2005). Visual prey capture in larval zebrafish is controlled by identified reticulospinal neurons downstream of the tectum. *J. Neurosci.* **25,** 9294–9303.

Gasparini, S., Losonczy, A., Chen, X., Johnston, D., and Magee, J. C. (2007). Associative pairing enhances action potential back-propagation in radial oblique branches of CA1 pyramidal neurons. *J. Physiol.* **580,** 787–800.

Göbel, W., Kampa, B. M., and Helmchen, F. (2007). Imaging cellular network dynamics in three dimensions using fast 3D laser scanning. *Nat. Methods* **4,** 73–79.

González, S., and Tannous, Z. (2002). Real-time, *in vivo* confocal reflectance microscopy of basal cell carcinoma. *J. Am. Acad. Dermatol.* **47,** 869–874.

Guntupalli, R., Haganb, V., Cooper, A., and Simpson, R. (2005). New ultra-high speed CCD camera achieves sub-electron read noise using on-chip multiplication gain (EMCCD) technology. *Proc. SPIE* **5580,** 905–912.

Hale, M. E., Ritter, D. A., and Fetcho, J. R. (2001). A confocal study of spinal interneurons in living larval zebrafish. *J. Comp. Neurol.* **437,** 1–16.

Hansma, H. G., and Hoh, J. H. (1994). Biomolecular imaging with the atomic force microscope. *Annu. Rev. Biophys. Biomol. Struct.* **23,** 115–140.

Heim, N., Garaschuk, O., Friedrich, M. W., Mank, M., Milos, R. I., Kovalchuk, Y., Konnerth, A., and Griesbeck, O. (2007). Improved calcium imaging in transgenic mice expressing a troponin C-based biosensor. *Nat. Methods* **4,** 127–129.

Hell, S. H., and Wichmann, J. (1994). Breaking the diffraction resolution limit by stimulated emission: Stimulated-emission-depletion fluorescence microscopy. *Opt. Lett.* **19,** 780–782.

Hell, S. W. (2007). Far-field optical nanoscopy. *Science* **316,** 1153–1158.

Helmchen, F., and Denk, W. (2005). Deep tissue two-photon microscopy. *Nat. Methods* **2,** 932–940.

Hernandez-Cruz, A., Sala, F., and Adams, P. R. (1990). Subcellular calcium transients visualized by confocal microscopy in a voltage-clamped vertebrate neuron. *Science* **247,** 858–862.

Higashijima, S., Hotta, Y., and Okamoto, H. (2000). Visualization of cranial motor neurons in live transgenic zebrafish expressing green fluorescent protein under the control of the islet-1 promoter/enhancer. *J. Neurosci.* **20,** 206–218.

Holtmaat, A. J., Trachtenberg, J. T., Wilbrecht, L., Shepherd, G. M., Zhang, X., Knott, G. W., and Svoboda, K. (2005). Transient and persistent dendritic spines in the neocortex *in vivo*. *Neuron* **45,** 279–291.

Hui, C. S., Bidasee, K. R., and Besch, H. R., Jr. (2001). Effects of ryanodine on calcium sparks in cut twitch fibres of Rana temporaria. *J. Physiol.* **534,** 327–342.

Iyer, V., Hoogland, T. M., and Saggau, P. (2006). Fast functional imaging of single neurons using random-access multiphoton (RAMP) microscopy. *J. Neurophysiol.* **95,** 535–545.

Jagger, D. J., and Housley, G. D. (2003). Membrane properties of type II spiral ganglion neurones identified in a neonatal rat cochlear slice. *J. Physiol.* **552,** 525–533.

Jang, K. E., and Ye, J. C. (2007). Single channel blind image deconvolution from radially symmetric blur kernels. *Opt. Express* **15,** 3791–3803.

Jenkins, D. E., Hornig, Y. S., Oei, Y., Dusich, J., and Purchio, T. (2005). Bioluminescent human breast cancer cell lines that permit rapid and sensitive *in vivo* detection of mammary tumors and multiple metastases in immune deficient mice. *Breast Cancer Res.* **7,** R444–R454.

Jiang, W., and Ludtke, S. J. (2005). Electron cryomicroscopy of single particles at subnanometer resolution. *Curr. Opin. Struct. Biol.* **15,** 571–577.

Jontes, J. D., Buchanan, J., and Smith, S. J. (2000). Growth cone and dendrite dynamics in zebrafish embryos: Early events in synaptogenesis imaged *in vivo*. *Nat. Neurosci.* **3,** 231–237.

Karlsson, J., von Hofsten, J., and Olsson, P. E. (2001). Generating transparent zebrafish: A refined method to improve detection of gene expression during embryonic development. *Mar. Biotechnol.* **3,** 522–527.

Kellermayer, M. S., Karsai, A., Kengyel, A., Nagy, A., Bianco, P., Huber, T., Kulcsár, A., Niedetzky, C., Proksch, R., and Grama, L. (2006). Spatially and temporally synchronized atomic force and total internal reflection fluorescence microscopy for imaging and manipulating cells and biomolecules. *Biophys. J.* **91,** 2665–2677.

Kerr, J. N., Greenberg, D., and Helmchen, F. (2005). Imaging input and output of neocortical networks *in vivo*. *Proc. Natl. Acad. Sci. USA* **102,** 14063–14068.

Klein, C., Pillot, T., Chambaz, J., and Drouet, B. (2003). Determination of plasma membrane fluidity with a fluorescent analogue of sphingomyelin by FRAP measurement using a standard confocal microscope. *Brain Res. Brain Res. Protoc.* **11,** 46–51.

Knight, M. M., Roberts, S. R., Lee, D. A., and Bader, D. L. (2003). Live cell imaging using confocal microscopy induces intracellular calcium transients and cell death. *Am. J. Physiol. Cell Physiol.* **284,** C1083–C1089.

Knott, G. W., Holtmaat, A., Wilbrecht, L., Welker, E., and Svoboda, K. (2006). Spine growth precedes synapse formation in the adult neocortex *in vivo*. *Nat. Neurosci.* **9,** 1117–1124.

Kockskamper, J., Sheehan, K. A., Bare, D. J., Lipsius, S. L., Mignery, G. A., and Blatter, L. A. (2001). Activation and propagation of Ca(2+) release during excitation-contraction coupling in atrial myocytes. *Biophys. J.* **81,** 2590–2605.

Korkotian, E., Oron, D., Silberberg, Y., and Segal, M. (2004). Confocal microscopic imaging of fast UV-laser photolysis of caged compounds. *J. Neurosci. Methods* **133,** 153–159.

Koster, A. J., and Klumperman, J. (2003)).Electron microscopy in cell biology: Integrating structure and function*Nat. Rev. Mol. Cell Biol.* **4** (Suppl.), SS6–SS10.

Kuo, C., Coquoz, O., Troy, T. L., Xu, H., and Rice, B. W. (2007). Three-dimensional reconstruction of *in vivo* bioluminescent sources based on multispectral imaging. *J. Biomed. Opt.* **12,** 024007.

Lassen, B., and Malmsten, M. (1996). Competitive protein adsorption studied with TIRF and ellipsometry. *J. Colloid Interface Sci.* **179,** 470–477.

Lippincott-Schwartz, J., and Patterson, G. H. (2003). Development and use of fluorescent protein markers in living cells. *Science* **300,** 87–91.

Lipp, P., Lüscher, C., and Niggli, E. (1996). Photolysis of caged compounds characterized by ratiometric confocal microscopy: A new approach to homogeneously control and measure the calcium concentration in cardiac myocytes. *Cell Calcium* **19,** 255–266.

Lister, J. A., Robertson, C. P., Lepage, T., Johnson, S. L., and Raible, D. W. (1999). Nacre encodes a zebrafish microphthalmia related protein that regulates neural-crest-derived pigment cell fate. *Development* **126,** 3757–3767.

Liu, K. S., and Fetcho, J. R. (1999). Laser ablations reveal functional relationships of segmental hindbrain neurons in zebrafish. *Neuron* **23,** 325–335.

Livet, J., Weissman, T. A., Kang, H., Draft, R. W., Lu, J., Bennis, R. A., Sanes, J. R., and Lichtman, J. W. (2007). Transgenic strategies for combinatorial expression of fluorescent proteins in the nervous system. *Nature* **450,** 56–62.

Lopez-Lopez, J. R., Shacklock, P. S., Balke, C. W., and Wier, W. G. (1994). Local, stochastic release of $Ca^{2+}$in voltage-clamped rat heart cells: Visualization with confocal microscopy. *J. Physiol.* **480,** 21–29.

Lumpkin, E. A., and Hudspeth, A. J. (1995). Detection of $Ca^{2+}$entry through mechanosensitive channels localizes the site of mechanoelectrical transduction in hair cells. *Proc. Natl. Acad. Sci. USA* **92,** 10297–10301.

Maierhofer, C., Gangnus, R., Diebold, J., and Speicher, M. R. (2003). Multicolor deconvolution microscopy of thick biological specimens. *Am. J. Pathol.* **162,** 373–379.

Majewska, A., Yiu, G., and Yuste, R. (2000). A custom-made two-photon microscope and deconvolution system. *Pflugers Arch.* **441,** 398–408.

Manz, W., Arp, G., Schumann-Kindel, G., Szewzyk, U., and Reitner, J. (2000). Widefield deconvolution epifluorescence microscopy combined with fluorescence in situ hybridization reveals the spatial arrangement of bacteria in sponge tissue. *J. Microbiol. Methods* **40,** 125–134.

McNally, J. G., Karpova, T., Cooper, J., and Conchello, J. A. (1999). Three-dimensional imaging by deconvolution microscopy. *Methods* **19,** 373–385.

Minsky, M. (1988). Memoir on inventing the confocal scanning microscope. *Scanning* **10,** 128–138.

Nägerl, U. V., Eberhorn, N., Cambridge, S. B., and Bonhoeffer, T. (2004). Bidirectional activity-dependent morphological plasticity in hippocampal neurons. *Neuron* **44,** 759–767.

Naora, H. (1955). Microspectrophotometry of cell nucleus stained by Feulgen reaction I. Microspectrophotometric apparatus without Schwarzschild-Villiger effect. *Exp. Cell Res.* **8,** 259–278.

Nasevicius, A., and Ekker, S. C. (2000). Effective targeted gene 'knockdown' in zebrafish. *Nat. Genet.* **26,** 216–220.

Ohara-Imaizumi, M., Nishiwaki, C., Kikuta, T., Nagai, S., Nakamichi, Y., and Nagamatsu, S. (2004). TIRF imaging of docking and fusion of single insulin granule motion in primary rat pancreatic beta-cells: Different behaviour of granule motion between normal and Goto-Kakizaki diabetic rat beta-cells. *Biochem. J.* **381,** 13–18.

Oheim, M., Beaurepaire, E., Chaigneau, E., Mertz, J., and Charpak, S. (2001). Two-photon microscopy in brain tissue: Parameters influencing the imaging depth. *J. Neurosci. Methods* **111,** 29–37.

O'Malley, D. M. (1994). Calcium permeability of the neuronal nuclear envelope: Evaluation using confocal volumes and intracellular perfusion. *J. Neurosci.* **14,** 5741–5758.

O'Malley, D. M., Kao, Y.-H., and Fetcho, J. R. (1996). Imaging the functional organization of zebrafish hindbrain segments. *Neuron* **17,** 1145–1155.

O'Malley, D. M., Sankrithi, N. S., Borla, M. A., Parker, S., Banden, S., Gahtan, E., and Detrich, H. W. (2004). Optical physiology and locomotor behaviors of wild-type and nacre zebrafish. *In* The Zebrafish: Cellular and Molecular Biology, (H. W. Detrich, M. Westerfield, and L. I. Zon, eds.) Academic Press, San Diego, CA.

O'Malley, D. M., Zhou, Q., and Gahtan, E. (2003). Probing neural circuits in the zebrafish: A suite of optical techniques. *Methods* **30,** 49–63.

Orger, M. B., Kampff, A. R., Severi, K. E., Bollmann, J. H., and Engert, F. (2008). Control of visually guided behavior by distinct populations of spinal projection neurons. *Nat. Neurosci.* **11,** 327–333.

Parker, I., Zang, W. J., and Wier, W. G. (1996). $Ca^{2+}$sparks involving multiple $Ca^{2+}$release sites along Z-lines in rat heart cells. *J. Physiol.* **497,** 31–38.

Park, M. K., Lomax, R. B., Tepikin, A. V., and Petersen, O. H. (2001). Local uncaging of caged Ca(2+) reveals distribution of Ca(2+)-activated Cl(-) channels in pancreatic acinar cells. *Proc. Natl. Acad. Sci. USA* **98,** 10948–10953.

Partridge, M. A., and Marcantonio, E. E. (2006). Initiation of attachment and generation of mature focal adhesions by integrin-containing filopodia in cell spreading. *Mol. Biol. Cell* **17,** 4237–4248.

Pawley, J. B. (2006). Handbook of Confocal Microscopy 3rd edn. Springer, New York, NY.

Perkins, B. D., Kainz, P. M., O'Malley, D. M., and Dowling, J. E. (2002). Transgenic expression of a GFP-rhodopsin C-terminal fusion protein in zebrafish rod photoreceptors. *Vis. Neurosci.* **19,** 257–264.

Photowala, H., Freed, R., and Alford, S. (2005). Location and function of vesicle clusters, active zones and $Ca^{2+}$channels in the lamprey presynaptic terminal. *J. Physiol.* **569,** 119–135.

Piston, D. W. (2005). When two is better than one: Elements of intravital microscopy. *PLoS Biol.* **3,** e207.

Pratusevich, V. R., and Balke, C. W. (1996). Factors shaping the confocal image of the calcium spark in cardiac muscle cells. *Biophys. J.* **71,** 2942–2957.

Reichert, W. M., and Truskey, G. A. (1990). Total internal reflection fluorescence (TIRF) microscopy. I. Modelling cell contact region fluorescence. *J. Cell Sci.* **96,** 219–230.

Rust, M. J., Bates, M., and Zhuang, X. (2006). Sub-diffraction-limit imaging by stochastic optical reconstruction microscopy (STORM). *Nat. Methods* **3,** 793–795.

Salmon, E. D., and Tran, P. (1998). High-resolution video-enhanced differential interference contrast (VE-DIC) light microscopy. *Methods Cell Biol.* **56,** 153–184.

Sarder, P., and Nehorai, A. (2006). Deconvolution methods for 3-D fluorescence microscopy images. *Signal Process. Mag. IEEE* **23,** 32–45.

Scheuss, V., Yasuda, R., Sobczyk, A., and Svoboda, K. (2006). Nonlinear $[Ca^{2+}]$ signaling in dendrites and spines caused by activity-dependent depression of $Ca^{2+}$extrusion. *J. Neurosci.* **26,** 8183–8194.

Schrader, M., Hell, S. W., and van der Voort, H. T. M. (1996). Potential of confocal microscopes to resolve in the 50–100 nm range. *Appl. Phys. Lett.* **69,** 3644–3646.

Serbus, L. R., Cha, B. J., Theurkauf, W. E., and Saxton, W. M. (2005). Dynein and the actin cytoskeleton control kinesin-driven cytoplasmic streaming in Drosophila oocytes. *Development* **132,** 3743–3752.

Shcherbo, D., Merzlyak, E. M., Chepurnykh, T. V., Fradkov, A. F., Ermakova, G. V., Solovieva, E. A., Lukyanov, K. A., Bogdanova, E. A., Zaraisky, A. G., Lukyanov, S., and Chudakov, D. M. (2007). Bright far-red fluorescent protein for whole-body imaging. *Nat. Methods* **4,** 741–746.

Sheppard, C. J. R., and Choudhury, A. (1977). Image formation in the scanning microscope. *Opt. Acta* **24,** 1051–1073.

Sieber, J. J., Willig, K. I., Kutzner, C., Gerding-Reimers, C., Harke, B., Donnert, G., Rammner, B., Eggeling, C., Hell, S. W., Grubmuller, H., and Lang, T. (2007). Anatomy and dynamics of a supramolecular membrane protein cluster. *Science* **317,** 1072–1076.

Sluder, G., and Wolf, D. E. (2007). Digital Microscopy. *Methods Cell Biol.* **81,** 1–608.

Smith, N., Coates, C., Giltinan, A., Howard, J., O'Connor, A., O'Driscoll, S., Hauser, M., and Wagner, S. (2004). EMCCD technology and its impact on rapid low-light photometry. *Proc. SPIE* **5499,** 162–172.

Stosiek, C., Garaschuk, O., Holthoff, K., and Konnerth, A. (2003). *In vivo* two-photon calcium imaging of neuronal networks. *Proc. Natl. Acad. Sci. USA* **100,** 7319–7324.

Strohmaier, A. R., Porwol, T., Acker, H., and Spiess, E. (2000). Three-dimensional organization of microtubules in tumor cells studied by confocal laser scanning microscopy and computer-assisted deconvolution and image reconstruction. *Cells Tissues Organs* **167,** 1–8.

Stuart, G. J., Dodt, H. U., and Sakmann, B. (1993). Patch-clamp recordings from the soma and dendrites of neurons in brain slices using infrared video microscopy. *Pflugers Arch.* **423,** 511–518.

Sun, D. A., Sombati, S., and DeLorenzo, R. J. (2001). Glutamate injury-induced epileptogenesis in hippocampal neurons: An *in vitro* model of stroke-induced ''epilepsy. *Stroke* **32,** 2344–2350.

Svoboda, K., Denk, W., Kleinfeld, D., and Tank, D. W. (1997). *In vivo* dendritic calcium dynamics in neocortical pyramidal neurons. *Nature* **385,** 161–165.

Svoboda, K., Tank, D. W., and Denk, W. (1996). Direct measurement of coupling between dendritic spines and shafts. *Science* **272,** 716–719.

Taylor, D. L., and Salmon, E. D. (1989). Basic fluorescence microscopy. *Methods Cell Biol.* **29,** 207–237.

Valkenburg, J. A., Woldringh, C. L., Brakenhoff, G. J., van der Voort, H. T., and Nanninga, N. (1985). Confocal scanning light microscopy of the Escherichia coli nucleoid: Comparison with phase-contrast and electron microscope images. *J. Bacteriol.* **161,** 478–483.

Varadi, A., Ainscow, E. K., Allan, V. J., and Rutter, G. A. (2002). Involvement of conventional kinesin in glucose-stimulated secretory granule movements and exocytosis in clonal pancreatic beta-cells. *J. Cell Sci.* **115,** 4177–4189.

Verveer, P. J., Gemkow, M. J., and Jovin, T. M. (1999). A comparison of image restoration approaches applied to three-dimensional confocal and wide-field fluorescence microscopy. *J. Microsc.* **193,** 50–61.

Verveer, P. J., Swoger, J., Pampaloni, F., Greger, K., Marcello, M., and Stelzer, E. H. (2007). High-resolution three-dimensional imaging of large specimens with light sheet-based microscopy. *Nat. Methods* **4,** 311–313.

Wako, T., Fukuda, M., Furushima-Shimogawara, R., Belyaev, N. D., Turner, B. M., and Fukui, K. (1998). Comparative analysis of topographic distribution of acetylated histone H4 by using confocal microscopy and a deconvolution system. *Anal. Chim. Acta* **365,** 9–17.

Wallace, W., Schaefer, L. H., and Swedlow, J. R. (2001). A workingperson's guide to deconvolution in light microscopy. *BioTechniques* **31,** 1076–1097.

Wang, H., Peca, J., Matsuzaki, M., Matsuzaki, K., Noguchi, J., Qiu, L., Wang, D., Zhang, F., Boyden, E., Deisseroth, K., Kasai, H., Hall, W. C., *et al.* (2007).High-speed mapping of synaptic connectivity using photostimulation in Channelrhodopsin-2 transgenic mice*Proc. Natl. Acad. Sci. USA* **104,** 8143–8148.

Wang, J., Wang, X., Irnaten, M., Venkatesan, P., Evans, C., Baxi, S., and Mendelowitz, D. (2003). Endogenous acetylcholine and nicotine activation enhances GABAergic and glycinergic inputs to cardiac vagal neurons. *J. Neurophysiol.* **89,** 2473–2481.

Wang, S. Q., Song, L. S., Lakatta, E. G., and Cheng, H. (2001). $Ca^{2+}$signalling between single L-type $Ca^{2+}$channels and ryanodine receptors in heart cells. *Nature* **410,** 592–596.

Weissleder, R., and Ntziachristos, V. (2003). Shedding light onto live molecular targets. *Nat. Med.* **9,** 123–128.

Wetterwald, A., van der Pluijm, G., Que, I., Sijmons, B., Buijs, J., Karperien, M., Löwik, C. W., Gautschi, E., Thalmann, G. N., and Cecchini, M. G. (2002). Optical imaging of cancer metastasis to bone marrow: A mouse model of minimal residual disease. *Am. J. Pathol.* **160,** 1143–1153.

Williams, R. M., Piston, D. W., and Webb, W. W. (1994). Two-photon molecular excitation provides intrinsic 3-dimensional resolution for laser-based microscopy and microphotochemistry. *FASEB J.* **8,** 804–813.

Willig, K. I., Rizzoli, S. O., Westphal, V., Jahn, R., and Hell, S. W. (2006). STED microscopy reveals that synaptotagmin remains clustered after synaptic vesicle exocytosis. *Nature* **440,** 935–939.

Wu, L., Lo, P., Yu, X., Stoops, J. K., Forghani, B., and Zhou, Z. H. (2000). Three-dimensional structure of the human herpesvirus 8 capsid. *J. Virol.* **74,** 9646–9654.

Xu, C., Zipfel, W., Shear, J. B., Williams, R. M., and Webb, W. W. (1996). Multiphoton fluorescence excitation: New spectral windows for biological nonlinear microscopy. *Proc. Natl. Acad. Sci. USA* **93,** 10763–10768.

Yasuda, R., Nimchinsky, E. A., Scheuss, V., Pologruto, T. A., Oertner, T. G., Sabatini, B. L., and Svoboda, K. (2004). Imaging calcium concentration dynamics in small neuronal compartments. *Sci. STKE* pl5.

Yu, S. P., O'Malley, D. M., and Adams, P. R. (1994). Regulation of M-Current by intracellular calcium in bullfrog sympathetic ganglion neurons. *J. Neurosci.* **14,** 3487–3499.

Zhou, Q., Godwin, D. W., O'Malley, D. M., and Adams, P. R. (1997). Visualization of calcium influx through channels that shape the *burst* and *tonic* firing modes of thalamic neurons. *J. Neurophys.* **77,** 2816–2825.

Zimmermann, T., Rietdorf, J., and Pepperkok, R. (2003). Spectral imaging and its applications in live cell microscopy. *FEBS Lett.* **546,** 87–92.